Enhanced functionality of low-affinity CD19 CAR T-cells is associated with activation priming and a polyfunctional cytokine phenotype

Ilaria M. Michelozzi[1], Eduardo Gomez Castaneda[1], Ruben V.C. Pohle[1], Ferran Cardoso Rodriguez[2], Jahangir Sufi[2], Pau Puigdevall Costa[3], Meera Subramaniyam[1], Si Wei Wu[1], Aleks Guvenel[1], Sara Ghorashian[4], Martin A. Pule[5], Christopher J. Tape[2], Sergi Castellano[3,6*], Persis J. Amrolia[1,7*] and Alice Giustacchini[1].

1. Molecular and Cellular Immunology Section, UCL Great Ormond Street Institute of Child Health, London, UK

2. Cell Communication Lab, Department of Oncology, University College London Cancer Institute, London, UK

3. Genetics and Genomic Medicine Programme, Great Ormond Street Institute of Child Health, University College London, London, UK

4. Department of Bone Marrow Transplant, Great Ormond Street Children's Hospital, London, UK.

5. Cancer Institute, University College London, London, UK

6. UCL Genomics, Great Ormond Street Institute of Child Health, University College London, London, UK

7. Departments of Bone Marrow Transplant and Haematology, Great Ormond Street Hospital for Children, London, UK

*These authors (S.C. and P.J.A.) contributed equally to this work

Corresponding author: Alice Giustacchini (a.giustacchini@ucl.ac.uk)

Abstract

We recently described a low-affinity second-generation CD19 chimeric antigen receptor (CAR, CAT) that showed enhanced expansion, cytotoxicity, and anti-tumour efficacy compared to the high-affinity (FMC63 based) CAR used in tisagenlecleucel, in pre-clinical models. Furthermore, CAT demonstrated an excellent toxicity profile, enhanced *in vivo* expansion, and long-term persistence in a Phase I clinical study. To understand the molecular mechanisms behind the improved properties of CAT CAR T-cells,

we performed a systematic *in vitro* characterization of the transcriptomic (RNA-seq) and protein (CyTOF) changes occurring in T-cells expressing low-affinity *vs* high-affinity CD19 CARs following stimulation with CD19-expressing cells. We demonstrate that CAT CAR T-cells show enhanced activation to CD19 stimulation and a distinct transcriptomic/protein profile with increased cytokine polyfunctionality post-stimulation compared with FMC63 CAR T-cells. Our results suggest that the enhanced functionality of low-affinity CAR T-cells may be sustained by the establishment of a self-reinforcing circuit activated through cytokines polyfunctional crosstalk.

Research Article

Introduction

T-cells genetically engineered to express CD19 chimeric antigen receptors (CAR T-cells) have shown remarkable efficacy in relapsed/refractory (r/r) B-cell malignancies leading to clinical licensing for r/r B-cell acute lymphoblastic leukaemia (B-ALL) and Non-Hodgkin Lymphoma.[1] Despite this success, several safety and efficacy hurdles remain[2]. CAR T-cells can trigger potent immune responses leading to transient but potentially life-threatening inflammatory events, such as cytokine release syndrome (CRS) and neurotoxicity[3,4]. CAR T-cell engraftment and expansion is a prerequisite for efficacy. Not all CD19 CAR T-cell products persist *in vivo* and long-term immune surveillance appears critical for preventing disease relapse, particularly in ALL. Thus, the design of versatile CAR T-cells, capable of balancing safety and efficacy, is contingent on our understanding of the molecular mechanisms underlying CAR T-cell function. The engagement of CARs to their cognate antigens results in the activation of CAR T-cells and promotes their rapid expansion as well as their differentiation into distinct T-cell subsets, mediating tumour cytolysis (effector cells) and providing long-lasting protection (memory cells). As tumour cell recognition by CAR T-cells relies on the binding of the CAR's single-chain variable fragment (scFv) to its epitope, fine-tuning the affinity of CARs to their antigens has become a strategy to modulate the strength of CAR T-cell responses[5].

The affinity of CARs is determined by their binding kinetics and the rates at which they associate to- and dissociate from their targets. The optimal affinity of a CAR is likely to vary depending on a number of factors, including the CAR design, the CAR expression levels and the antigen density on the target cells[6,7]. Chimeric immunoreceptors have an activation ceiling above which increasing the binding affinity does not improve T-cell activation but can rather result in T-cell exhaustion[8]. In contrast, by reducing CAR scFv affinity, the strength of the T-cell signal can be modulated, so that CAR T-cells discriminate different levels of antigen expression. CARs exhibiting slower antigen-association rates

to ErbB2, EGFR and CD123 targets showed reduced activation in response to low antigen concentrations, favouring differential targeting of tumour cells overexpressing the target *vs* normal tissue expressing the same target at physiological levels[8-10]. We have recently described a novel low-affinity CD19 CAR (CAT), with epitope, structure and stability similar to the widely used FMC63, but characterized by faster rates of antigen dissociation, leading to an overall 40-fold reduction of its affinity[6,11,12]. Pre-clinical testing of CAT CAR T-cells has revealed greater antigen-specific cytotoxicity, higher proliferation and more potent *in vivo* anti-tumour activity when compared to FMC63. In a Phase I clinical trial in patients with high-risk treatment-refractory paediatric B-ALL, CAT CAR T-cells resulted in lower toxicity in terms of severe CRS and displayed greater expansion than that reported for the FMC63 based tisagenlecleucel as well as excellent persistence[12]. In this regard, while CAT CAR T-cells have been designed to prevent excessive activation and reduce CRS and neurotoxicity risks, in line with other recently developed low-affinity CD19 CARs[13], enhancements in their cytotoxicity, expansion and persistence were unexpected[7] and the underlying molecular mechanisms to these functional phenotypes remain unknown.

The interaction between T-cell receptor (TCR) and the peptide-MHC complex offers however some insight on how immunoreceptors' affinity can dramatically influence T-cell functions[14]. Faster target off-rates in TCRs allow a single peptide-MHC complex to serially trigger several TCRs, resulting in amplified and sustained T-cell activation[14]. Similar to TCRs, low-affinity CARs may facilitate serial killing of target tumour cells, leading to enhanced activation and decreased exhaustion. Importantly, reduction of TCR avidity has been shown to also affect T-cell fate, with low-avidity TCRs promoting the expansion of self-renewing memory T-cell subsets[15]. Little is known about whether fine-tuning of CARs affinity influences T-cell fate in a similar fashion to TCRs, however, memory T-cell subsets are crucial for the establishment of long-term protection upon adoptive T-cell transfer, and their expansion in CAR T-cell products would be highly attractive[16,17]. Herein we perform a systematic *in vitro* characterization of the molecular and biochemical changes occurring in CAR T-cells, in response to a low-affinity CD19 CAR (CAT) as compared to a high-affinity one (FMC63). By combining bulk RNA sequencing with single-cell mass cytometry analyses (cytometry by time of flight, CyTOF), we show that the expression of the CAT CAR induces a memory-like activation priming in response to low concentrations of CD19-expressing B-cells found in the manufacture product. Upon antigen stimulation, we identified distinct molecular features downstream of CAT CAR activation responsible for enhancing CAT CAR T-cell functional response.

Results

Generation and quality assessments of low- (CAT) and high- (FMC63) affinity CD19 CARs from healthy donors

To dissect the molecular mechanisms behind the functional differences observed between low- (CAT) and high- (FMC63) affinity CD19 CAR T-cells[12], we interrogated transcript and protein expression readouts from T-cells lentivirally (LV) transduced with CD19 CARs differing only in their scFv (Supplementary Fig. 1a), before and after antigenic stimulation. In particular, we performed bulk transcriptomic analyses (RNA-seq) to identify CAR T-cell distinct gene expression signatures and mass cytometry analyses (CyTOF) to model at a single-cell resolution, differences in their downstream signalling. RNA-seq and CyTOF readouts from untransduced (UNTR) controls and T-cells LV transduced to express CAT or FMC63 CD19 CARs from healthy donors (HD1-HD8, Supplementary Table 1) were compared at baseline and following stimulation with CD19+ ALL cell line NALM6 (unstimulated and stimulated conditions, respectively), as schematized in Fig. 1a. Importantly, we ruled out significant differences in the transduction of the 2 CARs by fluorescence activated cell sorting (FACS), assessing the percentage of mCherry+ T-cells (LV fluorescent marker) across donors and experimental conditions. These ranged between 11.50 - 93.80% (median 48.55%) in FMC63 and 13.40 - 93.60% (median 43.60%) in CAT (Fig. 1b, top) and were thus comparable among individual HDs. Similarly, we excluded major differences in transgene expression between the 2 CARs by measuring mCherry mean fluorescent intensity (MFI), a proxy for CARs expression, in transduced T-cells (mCherry+) (Fig. 1b, top). These ranged between 8,277 – 21,578 (median 11,189) and 8,187 – 28,451 (median 10,843) in FMC63 and CAT, respectively, (Fig. 1b, top) and were comparable among individual donors. We also confirmed that both levels of LV transduction and transgene expression intensities remained comparable between constructs upon antigen stimulation (Fig. 1b, bottom). Finally, because the CD4/CD8 composition in CAR T-cell products can affect their anti-tumour activity *in vivo*[18], we compared the CD4:CD8 ratios in CAT and FMC63 CAR T-cells. While no difference was observed in the absence of antigen stimulation, upon NALM6 co-culture we found a slight but statistically significant reduction of CD4:CD8 ratio in CAT as compared to FMC63 (Fig. 1c). This variation was largely attributable to a relative decrease of the CD8+ fraction (and increase of CD4+) in FMC63 CAR T-cells after antigen stimulation (Fig. 1c and Supplementary Fig. 1b) as indicated by the similar frequencies observed in CAT and UNTR T-cells (Fig. 1c). These assessments confirmed that our CAR T-cell products were suitable to investigate the molecular features of CAT and FMC63 CAR T-cells.

135 **Low-affinity CD19 CAT CARs have higher activation priming in absence of antigen stimulation**
136
137 We next performed bulk RNA-seq of FACS-sorted UNTR T-cells (CD3+) and FMC63 or CAT CAR T-cells
138 (CD3+mCherry+) expanded for 4 days with or without stimulation with NALM6 at 2 time points (T1,
139 3h and T2, 24 h). Transcriptomic results confirmed that mCherry was an accurate proxy for CAR
140 transgene expression levels, as shown by the significant positive correlation between the MFI of
141 mCherry by FACS and the normalized RNA-seq counts aligning to the scFv region of each of the 2 CARs
142 (Fig. 2a) or to the exogenous sequence of mCherry (Supplementary Fig. 2a). Similarly, the proportion
143 of CD4 and CD8 T-cells detected by FACS was in line with the *CD4* and *CD8* mRNA levels
144 (Supplementary Fig. 2b and Fig. 2b). Principal component analysis (PCA) on the 500 most variable
145 expressed genes (top 100 genes shown in Supplementary Fig. 2c), distributed samples according to a
146 T-cell activation gradient (PC1, from UNTR to CAR activated samples), with the majority of variance in
147 gene expression across experimental conditions being explained by CD19-mediated CAR activation.
148 As expected, UNTR T-cells not expressing any CARs were mostly unaffected by antigen stimulation
149 (Fig. 2c). Similarly, PCA on protein expression from CyTOF, based on earth mover's distance (EMD)
150 scores (a sensitive measure of multivariate changes in protein levels)[19], and in the same experimental
151 conditions and timepoints than the gene expression, followed a similar gradient of sample activation,
152 shifting from UNTR samples to antigen stimulated CAR T-cells on PC1 (Fig. 2d and Supplementary Fig.
153 3a). Indeed, the 20 most variable genes upregulated upon stimulation with NALM6 in both FMC63 and
154 CAT CAR T-cells include genes involved in T-cell activation (*IL2RA*, *GZMB*) and proliferation (*PCNA*,
155 *LDHA*), which are expressed at very low levels in control T-cells (Fig. 2e and Supplementary Fig. 2c).
156 Consistent with this, the highest protein expression variation is from markers of T-cell activation
157 (CD25, NFAT1, HLA-DR) and proliferation (pRB) (Supplementary Fig. 3b). Of note in both RNA and
158 protein analyses unstimulated CAR T-cells show an intermediate RNA/protein expression profile
159 between UNTR and stimulated CAR T-cells. This suggests that CAR expression on its own in absence
160 of antigen stimulation induces basal T-cell activation (Fig. 2c-e). Importantly, unstimulated CAT
161 samples appear closer to antigen stimulated CAR T-cells than unstimulated FMC63, as well as having
162 less overlap with UNTR samples.
163
164 To gain further insights into the intermediate activation state observed in unstimulated CAT, we fuzzy
165 clustered genes by their gene expression and classified individual samples into more than 1 cluster to
166 resolve intermediate cell states and trajectories (Fig. 2f and Supplementary Fig. 2d)[20]. We identified 2
167 clusters, highly enriched for either inactive T-cells (cluster 1, which includes UNTR samples) or antigen-
168 activated CAR T-cells (cluster 2, which includes stimulated CAR T samples) (Fig. 2f). Notably, the

169 probability of unstimulated CAT samples of belonging to cluster 2 (activated CAR T-cells) was
170 substantially higher than that of unstimulated FMC63 (4/6 HDs in CAT *vs* 0/6 HDs inFMC63), further
171 evidencing the functional proximity between unstimulated CAT and activated CAR T-cells. In this
172 regard, using gene set enrichment analyses (GSEA) on the Hallmark collection, we confirmed that
173 while antigen stimulated CAT and FMC63 CAR T-cells have similar enrichment for most of the gene
174 sets involved in immune functions and cell proliferation, in the absence of antigen stimulation CAT are
175 uniquely enriched for T-cell activation pathways (Myc Targets V1, Hedghog signalling, Inflammatory
176 response, Interferon α response) (Fig. 2g). Altogether, these results support that unstimulated CAT
177 CAR T-cells have stronger T-cell activation priming prior to antigenic stimulation.

178 **Low-affinity CD19 CAT CAR activation priming is associated with and may be driven by residual**
179 **CD19-expressing B-cells**

180 To investigate whether the introduction of high- or low-affinity CD19 CARs can differentially affect
181 gene expression patterns in T-cells, we directly compared the transcriptome of FMC63 and CAT CAR
182 T-cells, in absence of antigen stimulation. Following differential gene expression (DGE) analysis, we
183 found that only 10 genes were significantly DE between these two conditions (FDR < 0.1,
184 Supplementary Table 2), 9 of which were upregulated in CAT *vs* FMC63 CAR T-cells. Among those, we
185 found genes involved in cytotoxicity (*GNLY*, *GZMK*) and markers of T-cell activation such as MHC class
186 II molecules (MHCII) (*HLA-DRA* and *HLA-DPA*) (Fig. 3a). This supports our previous observation of gene
187 expression in unstimulated CAT resembling more that of antigen activated CAR T-cells than gene
188 expression in unstimulated FMC63 (Fig. 2c). Mass cytometry analyses using a panel of antibodies
189 against markers of T-cell activation (Supplementary Table 3), confirmed that while unstimulated
190 FMC63 and CAT CAR T-cells showed similar EMD scores for the majority of the proteins investigated
191 (Supplementary Fig. 4a), unstimulated CAT CAR T-cells have significantly stronger activation priming
192 with higher expression of Granzyme B and CD25 ($p < 0.05$) (Fig. 3b). Antigen-independent CAR
193 activation, also known as tonic signalling, has been associated with CAR T-cell accelerated
194 differentiation and exhaustion, resulting in impaired anti-tumour efficacy *in vivo*[21-23]. To determine if
195 the activation priming observed in unstimulated CAT CAR T-cells was a consequence of CAR signalling
196 due to residual CD19 expressing cells during manufacture or tonic antigen-independent signalling, we
197 tested whether residual CD19+ B-lymphocytes were detectable in the CAR T-cell product and a
198 potential source of antigen specific activation. We monitored the proportion of CD19+ B-lymphocytes
199 in culture at different timepoints. While B-cells were detectable at day 0 in all samples (5.97% of cells
200 on average), at day 8 (5 day stimulation with CD3/CD28 beads + 3 day rest) they could only be detected
201 in the UNTR condition (1.43% of cells on average), and had been completely depleted from both CAR

202 constructs, as shown by FlowSOM analysis of mass cytometry data, clustering single-cells by cell types,
203 and the relative frequencies (Fig. 3c and Supplementary Fig. 4b)[24].
204
205 As both CARs were equally capable of clearing CD19-expressing B-cells found at low-ratio in the
206 manufacture product, we investigated whether the stronger activation in low- *vs* high-affinity CARs at
207 both RNA and protein levels resulted from distinct T-cell differentiation responses of these CAR T-cells
208 to CD19-priming. For instance, low receptor affinity and avidity in TCRs have been suggested to
209 preferentially promote differentiation into memory subsets and to favour T-cell persistence *in*
210 *vivo*[15,25]. Interestingly, CAT CAR T-cells exhibited a substantial increase in the fraction of CD8 central
211 memory T-cells (T_{CM}, CD62+CD45RA-) by FACS as compared to both UNTR and FMC63 conditions (Fig.
212 3d top). In addition, when using the gene signature-based method xCell to computationally infere
213 immune cell type composition from our gene expression profiles, we were able to confirm the
214 enrichment in CD8 T_{CM} in unstimulated CAT CAR T-cells compared to FMC63 (Fig. 3d bottom)[26]. This
215 suggests that CAR T-cells activation in response to residual B-lymphocytes present during the
216 manufacture may preferentially induce a T_{CM} phenotype in low-affinity CAT CAR T-cells.

217 **CD19 stimulation of low-affinity CAT CAR T-cells results in a distinct transcriptomic and protein**
218 **profile than high-affinity FMC63 CAR T-cells with enhanced activation/proliferation**
219
220 We next assessed the impact of "activation priming" and the increased proportion of T_{CM} on the
221 molecular response to antigen stimulation of unstimulated CAT CAR T-cells. Importantly, the stronger
222 basal activation observed in these cells did not prevent an even stronger response when exposed to
223 CD19-expressing NALM6, as shown by a greater increase than FMC63 in the expression of activation,
224 proliferation and cytotoxic markers, relatively to the unstimulated constructs (Supplementary Fig. 5
225 and 6). In agreement, after 24 h stimulation with NALM6, we identified 51 DE genes, 35 of which were
226 upregulated in CAT compared to FMC63 (Fig. 4a and Supplementary Table 4). CD19 stimulation in CAT
227 CAR T-cells also led to significantly augmented expression of immune stimulatory/proliferation
228 cytokines (*IFNG, CSF2, CXCL8*), and IFN-γ responsive genes (*CIITA*) (Fig. 4a and Supplementary Fig. 7a).
229 Conversely, CAT CAR T-cells displayed significantly decreased expression of the genes encoding for
230 CRIF1 (*GADD45GIP1*), an inhibitor of cell cycle progression, and for FOXP3, the Treg-associated
231 transcription factor known to be only transiently expressed in the initial stages of Th1 response and
232 rapidly downregulated afterwards[27,28] (Fig. 4a). These results suggest that following antigenic
233 stimulation CAT CAR T-cells show a different transcriptomic profile resulting in stronger activation and
234 proliferation than stimulated FMC63. These observations were further substantiated at the protein
235 level. Indeed, among the markers investigated (Supplementary Fig. 7b), CAT CAR T-cells exhibited a

236 marked increase in the expression (as measured by EMD score) of CD25 and NFAT1, indicators of T-
237 cell activation.
238
239 In addition to a significant increment of pRB and CD8 in CAT CAR T-cells, indicating an increased
240 fraction of proliferating CD8+ CAR T-cells, we noted enhanced expression of the IL7 receptor (CD127),
241 commonly associated to memory T-cell phenotypes[29,30] (Fig. 4b). Moreover, the augmented gene
242 expression of the MHCII trans-activator CIITA observed in CAT, resulted in a corresponding trend
243 toward the increase of HLA-DR protein[31,32] (Fig. 4b). Interestingly, in addition to being known as late
244 markers of T-cell activation, MHCII molecules have also been suggested to play a role in T-cell-T-cell
245 contact, potentially leading to the reinforcement of the immune response[33]. Additionally, CAT CAR T-
246 cells showed increased expression of the *TNFSF4* gene (Fig. 4a), encoding for the ligand of the T-cell
247 co-stimulatory receptor OX40 (OX40L). While OX40L is mainly expressed by antigen presenting cells
248 to promote T-cell activation during antigenic stimulation, it is also expressed in activating T-cells,
249 where leads to a homotypic OX40L-OX40 signalling axis promoting T-cell longevity and memory
250 differentiation[34]. Further, we also noted the increased expression of the inflammatory chemokine
251 genes *CCL4* and *CCL3L1* and genes involved in cell migration (*FLT1*, *DOCK5*) and focal adhesion
252 (*COL6A3*) in stimulated CAT CAR T-cells (Supplementary Fig. 7a). Importantly, the secretion of CCL4
253 and CCL3 by activated T-cells has been shown to mediate T-cell attraction toward one another,
254 promoting T-cell clusters formation and synaptic cytokines exchange coordinating immune
255 responses[35-38]. These results suggest that homotypic interactions between CAT CAR T-cells may play a
256 role in the enhanced activation/proliferation observed following CD19 antigenic stimulation
257 compared with FMC63 CAR T-cells.
258
259 **The enhanced functionality of low-affinity CD19 CAR T-cells is associated to a distinct cytokine**
260 **polyfunctional phenotype upon antigen stimulation**
261
262 To identify the mechanism underlying the stronger activation of CAT CAR T-cells, we next analysed
263 their cytokine production at the single-cell level by mass cytometry. We focused our analysis on T1 (3
264 h stimulation) as it recapitulates the median expression peak of cytokines in stimulated T-cells[39]. The
265 overall protein intensities measured by EMD scores (Supplementary Fig. 8a) indicated an increased
266 expression of Granzyme B (also observed in unstimulated CAT *vs* FMC63, Fig. 3b) and a trend toward
267 the upregulation of additional effector cytokines (IFN-γ, TNF-α) and of immune stimulatory molecules
268 (GM-CSF and IL-2). No upregulation was observed for Th2/immune-modulatory cytokines (IL-4, IL-5
269 and TGF-ß) and for Perforin B (Supplementary Fig. 8b). Because most individual differences in cytokine

levels were not statistically significant, we investigated the overall pattern of cytokine co-expression in CAT and FMC63 CAR T-cell responses. The ability of a single T-cell to express simultaneously more than 1 cytokine (polyfunctionality) has been linked to productive immune responses[40,41] and more recently described as a distinctive feature of CAR T-cells correlating with their improved anti-tumour efficacy[42,43]. We measured the frequency at which the 12 cytokines included in our analysis were co-expressed in single CAR T-cells, thus providing a comprehensive profile of their cytokine polyfunctionality. Upon stimulation with NALM6, 30.10% of FMC63 and 45.26% of CAT CAR T-cells were polyfunctional. Furthermore, not only the frequency of polyfunctional CAR T-cells, but also the number of cytokines co-expressed was higher in CAT than in FMC63, with a marked increment in the proportion of cells expressing combinations of 3 or more cytokines (7.33% in FMC63 *vs* 17.50% in CAT) (Fig. 5a). Importantly, a robust increase in CAT CAR T-cell cytokine polyfunctionality was only observed upon CD19 stimulation, in support of the antigenic specificity of the response (Fig. 5a, b and Supplementary Fig. 9a, b). The polyfunctional profiles of stimulated CAT CAR products were dominated by combinations of cytokines involving the effector molecules TNF-α, IL-2 and Granzyme B (Fig. 5b). Among all the possible combinations analysed, the cytokine co-expression patterns significantly enriched in CAT *vs* FMC63 involved effector (IFN-γ, TNF-α, Granzyme B), stimulatory (IL-2, GM-CSF) and T-cell memory-associated (IL-23)[44] cytokines (Fig. 5c).

p38 MAPK signalling axis is preferentially activated in response to low-affinity CD19 CAT CARs

To dissect the signalling axes resulting from for FMC63 and CAT differential cytokine profiles, we analysed the intracellular signalling of CAR T-cells using mass cytometry at 24 h post-stimulation. In particular, we measured the activation of mammalian Target of Rapamycin Complex 1 (mTORC1) dependent cell proliferation and protein translation signals, effectors of the TCR/CAR CD3ζ chain (pZAP70, pERK, pp38), and their downstream transcription factors (NFAT1, pCREB, FOXP3). To ensure that we only captured CAR dependent signals, CD3/CD28 beads were removed from the culture 48 h before NALM6 stimulation. Upon antigen stimulation, CAT significantly upregulated the mTORC1 downstream effectors pS6 and pRB ($p < 0.01$) (Fig. 6a), consistent with the increased proliferation observed in pre-clinical studies[12]. In addition, CAT CAR T-cells showed enhanced phosphorylation of ZAP70 (pZAP70) ($p < 0.05$) (Fig. 6a), a proximal effector of the CD3ζ chain (present in the CAR constructs Supplementary Fig. 1a) whose phosphorylation initiates the TCR intracellular signalling. Downstream of the pZAP70 cascade, the phosphorylated form of p38 mitogen activated protein kinase (MAPK) was upregulated in CAT CAR T-cells compared with FMC63 CAR T-cells ($p < 0.05$), while no difference was observed in the induction of another pZAP70 effector, pERK (Fig. 6a). Among the

304 transcription factors analysed, CAT CAR T-cells exhibited higher levels of NFAT1 and FOXP3
305 (Supplementary Fig. 10a). Of note, FOXP3 transient expression in T effectors (as demonstrated by its
306 concurrent transcript decrease, Fig. 4a) correlates with sustained levels of CD127, proliferation and
307 pro-inflammatory cytokine secretion[27].
308
309 To model CAT CAR downstream signalling network, we performed a density resampled estimate of
310 mutual information (DREMI) analysis[45] on our mass cytometry results. While EMD scores measure
311 intensity in individual proteins, DREMI scores quantify the intensity of interaction (direct or indirect)
312 between pairs of proteins. We focused on signalling differences between CAT and FMC63 and built
313 interaction networks centred on those differing molecules and connections. Up (red) and down (blue)
314 regulation of individual proteins, relative to the average protein expression in each condition, was
315 represented by EMD scores in the network nodes (circles in Fig. 6b, Supplementary Fig. 10b), while
316 interaction between two proteins was represented by DREMI scores (Supplementary Fig. 10c) in the
317 network edges (arrows in Fig. 6b, Supplementary Fig. 10b). While many of the signalling modules
318 identified showed similar activation, as expected from CD19 CARs only differing for their antigen
319 affinity (Supplementary Fig. 8a right), our analysis identified a signalling axis around p38 MAPK, which
320 was selectively upregulated in CAT upon antigen stimulation (Fig. 6b and Supplementary Fig. 10c). Of
321 note, p38 MAPK can be activated both downstream of CD3ζ chain stimulation (through pZAP70,
322 antigen-dependent activation) or in response to cytokines signalling (antigen-independent activation).
323 It is however only essential for cytokine-mediated activation in T-cells and thus of relevance to this
324 activation route in CAT CAR T-cells.[46,47] Further, p38 MAPK pathway regulates the stability and
325 translation of several anti-tumoural cytokine transcripts, including IL-2, IFN-γ, TNF-α, GM-CSF,
326 CXCL8,[48,49] some of which were upregulated at the mRNA and/or protein levels in CAT expressing CAR
327 T-cells (Fig. 4, Supplementary Fig. 8b). Lastly, the activation of p38 induces NFAT expression,
328 promoting its interaction with the coactivator CREB-binding protein and increased transcription of T-
329 cell activation genes, including cytokines. These results, combined with the marked polyfunctional
330 phenotype observed in CAT (Fig. 5), point to a self-reinforcing circuit of cytokine mediated activation
331 in CAT CAR T-cells, as depicted in Fig. 6c.

332 **Low-affinity CAT CAR T-cells display increased trogocytosis**

333 To determine the role of different T-cell subsets in the induction of cytokine polyfunctionality in CAT
334 CAR T-cells, we correlated the expression of cytokines and T-cell phenotypic surface markers, using
335 mass cytometry DREMI scores. Interestingly, among all the surface markers tested (Supplementary
336 Fig. 11a), CD19 (the CARs cognate antigen) established the greatest number of significant correlations

337 (with TNF-α, GM-CSF, IL-2 and TGF-β) in CAT CAR T-cells (Fig. 7a). Indeed FlowSOM analysis revealed
338 that CD19 expression was consistently detected in both CD4+ and CD8+ CAR T-cells (Fig. 7b). We
339 reasoned that if CD19 signal was originating from cell doublets (CAR T-NALM6), we should detect its
340 expression at both transcript and protein level. Interestingly, RNA-seq performed at 24 h after
341 stimulation had negligible expression of *CD19* and *CD22* (another B-cell marker), in contrast to *CD3*
342 mRNAs, arguing against the CD3+CD19+ signal originating from cell doublets (Supplementary Fig. 11b).
343 This observation was further substantiated by the absence of increase in DNA staining intensity
344 (marker of doublets) in the CD19+ CAR T-clusters by mass cytometry (Supplementary Fig. 11c). CD19
345 CAR T-cells have been recently reported to transiently expose CD19 cognate antigen on their surface
346 membrane, following target cell engagement. This process, trogocytosis, involves the transfer of
347 membrane fragments from antigen expressing cells to lymphocytes. As a consequence of CAR T-cells
348 becoming targets themselves, trogocytosis has been linked to fratricide killing in FMC63 CAR T-cells[50].
349
350 Our results highlighted a transient kinetic of the *bona fide* trogocytosis observed, peaking at 3 h after
351 NALM6 stimulation in both CAT and FMC63 (Fig. 7b, c), and decreasing after 24 h, while persisting only
352 in CAT CAR T-cells for longer (Fig. 7b, c and Supplementary Fig. 12a). The increased levels of
353 trogocytosis in CAT CAR T-cells suggests that engagements between CAT CAR T-cells and their targets
354 may be unusually frequent, consistent with the serial triggering pattern observed in low-affinity
355 immune receptors[14,51]. The longer persistence of CAT trog+ CAR T-cells in culture may result from
356 reduced fratricide since tumour cells (NALM6) expressed significantly higher levels of CD19 protein
357 than trog+ CAT CAR T-cells (Fig. 7d). As a result, trog+ CAR T-cells spared from fratricide killing may
358 serve as an additional source of CD19-dependent CAR T stimulation after NALM6 cells have been
359 cleared. To corroborate this hypothesis, we analysed trog+ CAR T-cell functional phenotypes by mass
360 cytometry at different timepoints after stimulation (Supplementary Fig. 12b). At 3h post-stimulation,
361 when CAT and FMC63 have similar frequencies of trog+ CAR T-cells, trog+ CAT CAR T-cells showed
362 higher markers of activation and cytokine polyfunctionality (Supplementary Fig. 12c, d). Strikingly, at
363 24 h after stimulation (when we observe no residual NALM6 in the co-culture, Fig. 7e), we noticed
364 that trog+ CAT CAR T-cells preserved a robust activation phenotype, with enhanced expression of
365 proliferation markers (pRB, CD3), T-cell activation factors (CD25, NFAT1, FOXP3), lytic cytokines
366 (Granzyme B, Perforin B) and p38 MAPK signalling (Fig. 7f and Supplementary Fig. 12e). Furthermore,
367 trog+ CAT CAR T-cells at 24 h maintained the ability to co-express combinations of effector (IFN-γ,
368 Granzyme B) and stimulatory (IL-2) cytokines. In contrast, trog+ FMC63 shifted to higher expression
369 of TGF-β (alone or in combination with other cytokines), which is commonly associated to the

370 abrogation of T-cell proliferation and cytotoxicity (Fig. 7g and Supplementary Fig. 12e). Altogether
371 these results point to a self-reinforcing role of trogocytosis in low-affinity CD19 CAT CAR T-cells.
372
373 **Discussion**
374
375 Modulating CAR T-cell affinity may enable us to enhance anti-tumour response and long-term tumour
376 surveillance, while minimizing CAR T-cell related toxicity. To this aim, understanding the molecular
377 determinants of treatment efficacy in low-affinity CARs is crucial to inform their design and optimize
378 their manufacture. We thus investigated the molecular features of low-affinity CD19 CAT CAR T-cells,
379 compared them with those of a high-affinity FMC63-based one, to begin unravelling the molecular
380 mechanism behind CAT clinical benefits[12]. In this regard, low-affinity CAT CARs induce stronger anti-
381 tumour responses than high-affinity ones, an apparent paradox, which could be explained by the
382 faster target off-rate of low-affinity CARs. Faster dissociation requires fewer targets to serially trigger
383 a larger number of CARs and amplify anti-tumoural response[14]. This would align with the proposed
384 model of temporal and spatial summation of T-cell activation, in which signals from serially triggered
385 immunoreceptors can be accumulated and integrated overtime to reach the threshold required for T-
386 cell activation[51]. Indeed, we found that residual B-cells expressing CD19 in the CAR T-cell product
387 prime both CAT and FMC63 CARs, with CAT however having a more pronounced expansion of CD8
388 T_{CM}. This is consistent with the hypothesis that CAT serial triggering may amplify T-cell activation from
389 lower antigen levels[14] and points to a boosting role of CD19 antigen priming during CAR T-cell
390 manufacture.
391
392 Our transcriptomic and protein profiling revealed that unstimulated CAT CAR T-cells are functionally
393 closer to antigen activated CAR T-cells than FMC63 CAR T-cells. It is not clear whether this "activation
394 priming" results from stimulation by residual CD19+ cells during manufacture or antigen-independent
395 CAR tonic signalling to their molecular phenotype. Mass cytometry analyses of unstimulated CAR T-
396 cells did not reveal activation of CAR-downstream signalling in CAT nor in FMC63, arguing against CAR-
397 dependent tonic signalling being responsible for CAT activation priming. On the other hand, the
398 transcriptomic profile of unstimulated CAT CAR T-cells, identified a number of upregulated activation
399 genes (*HLA-DBP1*, *HLA-DRA* etc). Despite these genes being commonly associated to T-cell activation,
400 their basal expression is also increased in memory T-cells as compared to $T_{NAÏVE}$ cells. This is because
401 memory T-cells are characterized by an open chromatin conformation favouring the access of
402 transcription factors to immune response genes, thus ensuring a pool of readily available mRNAs that
403 can be rapidly translated following stimulation[52]. When stimulated with CD19-expressing NALM6 cell

404 line, CAT CAR T-cells showed a distinct transcriptomic and protein response to CD19 antigenic
405 stimulation than FMC63 CAR T-cells with increased expression of proliferation, activation and
406 cytotoxic markers at both RNA and protein levels. *In vivo* clonal kinetics analyses have shown that
407 single CD19 CAR T-cells that have higher expression of cytotoxic related genes in the manufacture
408 product, many of which in common with ours (including *IFNG*, *HLA-DRA*, *CCL4*), gave rise to superior
409 *in vivo* expansion and survival, significantly contributing to later timepoints after adoptive transfer in
410 patients[53]. While we did not observe major differences in single cytokines, upon stimulation CAT CAR
411 T-cells were uniquely characterized by a polyfunctional pattern of cytokine expression, with a marked
412 increase in the frequency of single CAR T-cells expressing >=3 cytokines when compared to FMC63.
413 CAT polyfunctional profile was dominated by combinations of effector cytokines, consistent with their
414 potent anti-tumour activity. It has been recently shown that the ability of CAR T-cells to produce
415 multiple cytokines (polyfunctionality) in response to antigen exposure may be associated with
416 improved anti-tumour responses *in vivo*[42].
417
418 Analyses of intracellular signalling by mass cytometry revealed the increased phosphorylation of p38
419 MAPK in stimulated CAT as compared to FMC63. P38 MAPK is central to promoting mRNA stability of
420 proinflammatory genes which, intriguingly, may contribute to increased cytokine co-expression in
421 CAT. Furthermore, the activation of p38 can induce NFAT and pCREB-dependent transcription of T-
422 cell activation genes, including cytokines[48]. Analysis of gene expression also revealed the upregulation
423 of chemoattractive cytokines CCL4 and CCL3L1 in CAT, which induce T-cell homotypic interactions and
424 promote the reciprocal exchange of self-reinforcing signals such as OX40L,[34,37] which are upregulated
425 in CAT as well. These data suggest enhanced p38 MAPK phosphorylation in CAT CAR T-cells may play
426 a key role in establishing a self-reinforcing circuit of cytokine-mediated activation as depicted in Fig.
427 6c. In support, stimulated CAT CAR T-cells consistently formed larger clusters than FMC63 CAR T-cells
428 in culture (data not shown). T-cell aggregates are also instrumental in mediating the synaptic exchange
429 of cytokines, thus further amplifying and coordinating immune responses. Notably, cytokine crosstalk
430 among T-cells can trigger antigenic-independent stimulation and this T-cell activation route is
431 preferentially taken by memory T-cells as opposed to other T-cell subsets, due to their intrinsically
432 higher cytokine responsiveness[46]. Of note, p38 MAPK can be activated downstream of both antigen-
433 and cytokine- mediated stimulation through different mechanisms, but it is only indispensable for the
434 latter[14], suggesting a cause and effect relationship between the polyfunctional phenotype observed
435 and the activation of p38 MAPK signalling axis.
436

437 Finally, we associated the cytokine polyfunctional phenotype in CAT to CD19 trogocytosis in CAR T-
438 cells. Trogocytosis requires the uptake of the target antigen by T-cells and can result in either immune
439 suppression (T-cell anergy and fratricide killing), as recently shown for FMC63- based CARs[50], or
440 stimulation (increasing cytokine secretion and cell proliferation)[54]. Interestingly, we noted that the
441 proportion of CAT CAR T-cells undergoing trogocytosis (trog+) was higher than in FMC63 the longer
442 after stimulation. Considering that one unique property of low-affinity CAR T-cells is the ability to
443 selectively kill target cells with high levels of antigen (tumour cells) while sparing low antigen-
444 expressing cells (trog+ CAR T), it is tempting to speculate that reduced fratricide killing is responsible
445 for the increased persistence of trog+ CAT CAR T-cells in culture. We speculate that trogocytosed CD19
446 in CAT CAR T-cells may provide sustained intracellular signalling to CAT CAR T-cells between successive
447 short rounds of antigen ligation typical of low-affinity CARs, consistent with a previously proposed
448 model for the stimulatory role of trogocytosis in CD4 T-cells[55], enhancing activation of low-affinity CAR
449 T-cells. In conclusion, we describe the molecular mechanisms underlying the low-affinity CAT CAR T-
450 cell functional phenotype. We provide evidence that the potent and long-term anti-tumour responses
451 observed with low-affinity CAT CAR T-cells reflect a distinct pattern of both activation priming and
452 downstream signalling compared to high-affinity CD19 CAR T-cells which is established and sustained
453 in CAR T-cells by a self-reinforcing circuit activated via cytokines polyfunctional crosstalk. This work
454 may inform the future design of versatile CAR T-cells, capable of balancing safety, efficacy and long-
455 term persistence.
456

457 **Methods**

458

459 **Human peripheral blood samples and cell lines**

460

461 Peripheral blood was collected from 13 HDs after having obtained informed consent. Fresh
462 mononuclear cells were isolated by Ficoll density gradient centrifugation (day 0) and used for
463 experiments. All analyses were performed on fresh T- or CAR T-cells except for 96 h memory subset
464 FACS analysis. HD details and relative experimental procedure are reported in Supplementary Table
465 1. The human ALL cell line NALM6 was purchased from DSMZ. Cells were cultured according to
466 manufacturer's instructions in complete RPMI 1640 medium, GlutaMAX™ Supplement (Gibco™,
467 Thermo Fisher Scientific, Waltham, MA, USA) supplemented with 10% of heat-inactivated Foetal
468 Bovine Serum (FBS) (Gibco™, Thermo Fisher Scientific), 100 IU penicillin and 100 μg/ml streptomycin
469 (Sigma-Aldrich, St. Louis, MO, USA).
470

471 ***Ex vivo* T-cell expansion**

472

473 Freshly isolated PBMCs from HD1-HD8 were cultured in TexMACS™ medium (Miltenyi Biotec, Bergisch
474 Gladbach, Germany), an optimised T-cell medium. To induce T-cell expansion, CD3/CD28 beads (CTS™
475 Dynabeads™ CD3/CD28, Thermo Fisher Scientific) were added to cells in MACS GMP Cell
476 Differentiation Bags (Miltenyi Biotec) at a 1:3 lymphocyte:bead ratio. CD3/CD28 beads were
477 magnetically removed from the culture on day 5 and CAR T-cells rested for 48 h before proceeding to
478 antigen stimulation.

479

480 **CAR construct generation**

481

482 CD19 FMC63 and CAT CAR transfer vectors were generated as previously described[12] and were
483 provided by P.J.A.. The vector structure is schematised in Supplementary Fig. 1a.

484

485 **Lentiviral production by transient transfection**

486

487 Lentiviral production was performed by transient transfection according to the following procedure.
488 The day before transfection, 5.5 x 10^6 293T cells were seeded per 175 cm^2 flasks in complete DMEM,
489 high glucose, GlutaMAX™ Supplement (Gibco™, Thermo Fisher Scientific) supplemented with 10%
490 FBS.
491 To generate viral particles, 293T cells were co-transfected with second generation LV packaging
492 plasmids pMD2.G and pCMV-dR8.74 (plasmidFactory, Bielefeld, Germany) and CAR transfer vectors
493 using GeneJuice® Transfection Reagent (Merck-KGaA, Darmstadt, Germany) according to
494 manufacturer's recommendations. LV supernatants were collected at 48 and 72 h post-transfection,
495 pooled, filtered and stored at -80°C before use.

496

497 **Lentiviral transduction of T-cells**

498

499 Following overnight activation with CD3/CD28 beads, 0.5 x 10^6 beads-activated T-cells from HD1-HD8
500 were suspended in 0.5 ml of TexMACS, transduced to express CD19 CAR construct (FMC63 or CAT)
501 with 1 ml of LV supernatant in RetroNectin® (Takara Bio, Kusatsu, Shiga, Japan)-coated 24-well plates
502 and spinoculated at 1,000 g for 40 min at room temperature. Generally, 6-8 x 10^6 beads-activated T-
503 cells per donor per construct were seeded for transduction. Transduction efficiency was assessed by
504 FACS evaluating mCherry (LV fluorescent marker) expression, at day 8 (7 days after transduction).

505 UNTR beads-activated T-cells per each donor were used as a control throughout the experiment and
506 were subjected to the same experimental conditions as LV-transduced ones.
507
508 **NALM6 and CAR T-cells co-cultures**
509
510 To assess the anti-tumour activity of CD19 CAR T-cells, we set-up co-cultures with CD19-expressing
511 NALM6 for 3, 24 or 96 h (stimulated conditions) on day 7 (6 days after transduction and 2 days post-
512 CD3/CD28 beads removal). Briefly, beads-activated T-cells from HD1-HD8 were incubated for 48 h in
513 optimised T-cell medium before stimulation. 0.1 x 10^6 UNTR or FMC63 or CAT beads-activated T-cells
514 were seeded in 96-well plates in complete TexMACS medium in a 1:1 ratio with irradiated (40 Gy)
515 NALM6. Generally, 0.1-1.5 x 10^6 beads-activated T-cells per donor per condition (UNTR, FMC63 and
516 CAT) were stimulated.
517 Unstimulated, beads-activated T-cells per each donor, condition and time point were kept in culture
518 under the same experimental conditions as antigen-stimulated T-cells.
519
520 **Flow cytometry activated cell sorting and antibody staining**
521
522 All FACS experiments included Fluorescence minus one (FMO) and single-antibody stained BD™
523 CompBeads (BD Biosciences) controls to set expression threshold and to calculate compensation,
524 respectively. Live cells were selected based on their non-permeability and lack of fluorescence
525 associated with DAPI Solution (BD Biosciences, Franklin Lakes, NJ, USA). The combination of
526 monoclonal antibodies used to identify T-cell subsets is described in the main text. Following 24 or 96
527 h of stimulation, cells from HD1-HD8 in all the experimental conditions were labelled with BV510-anti
528 CD3 (clone OKT3), APC-CY7-anti CD4 (clone SK3), PerCP/CY5.5-anti CD8 (clone RPA-T8), AF647-anti
529 CD62L (clone DREG-56), BV785-anti CD45RA (clone HI100) (BioLegend, San Diego, CA, USA) in order
530 to detect CD4, CD8 and memory subsets within live T-/CAR T-lymphocytes. PBMCs from HD9-HD13
531 were labelled with PE-anti CD19 (clone HIB19; BioLegend) to detect B-cells within lymphocytes in the
532 samples soon after isolation. Experiments were performed on a cell sorter FACSAria™ III (BD
533 Biosciences) and on a CytoFLEX analyzer (Beckman Coulter Inc., Brea, CA, USA) and analysed with
534 FlowJo™ software v10.6.1 (BD Biosciences) and Cytobank platform (www.cytobank.org).
535
536 **RNA sequencing libraries preparation and sequencing**
537

538 RNA sequencing libraries were generated from 8 donors (HD1-HD8), across six experimental
539 conditions, UNTR T-cells or FMC63 or CAT CAR T-cells in either absence or presence of NALM6
540 (unstimulated or stimulated). 1,000 T-cells/CAR T-cells were FACS-sorted in single PCR tubes
541 containing 4 ul of QIAGEN lysis buffer from QIAseq FX Single Cell RNA Library Kit (QIAGEN, Hilden,
542 Germany) and stored at -80°C. The kit steps include reverse transcription, cDNA amplification and
543 PCR-free NGS library preparation. Libraries were purified using AMPure XP magnetic beads (Beckman
544 Coulter Inc.,) according to the manufacturer instructions. After beads purification the libraries were
545 resuspended in 50 µL of buffer EB (Qiagen) and stored at -20 °C. Size and concentration of the libraries
546 generated was assessed using High Sensitivity Bioanalyzer (Agilent, Santa Clara, CA, USA) and Qubit
547 High-Sensitivity DNA kit (Invitrogen™, Thermo Fisher Scientific), respectively. Libraries were
548 equimolarly pooled to a final concentration of 10 nM and were sequenced with Illumina HiSeq 3000
549 (150 bp pair-end reads) at UCL Genomics.

550

551 **RNA sequencing analysis**

552

553 Sequencing quality control and mapping was performed on Fedora 32. DGE analysis and downstream
554 analyses were performed in *R 4.0.2* on Windows 10 (build 18362). Additional details can be found in
555 the transcriptomic Supplementary Bioinformatics Material (SBM). An FDR smaller than 0.1 (when
556 multiple tests were performed) or a *P* value smaller than 0.05 (when only one test was performed)
557 was considered statistically significant. Quality control and adapters trimming was performed with
558 *FastQC 0.11.9*[56] and *cutadapt 2.10*[57]. Sequences were mapped with *STAR 2.7.3a*[58] to the release 31 of
559 the Human Genome (GRCh38.p12)[59] and summarised with *featureCounts* from the *subread 2.0.0*
560 software package[60]. Only genes annotated as protein-coding genes were included into the DE and
561 downstream analyses. These were further filtered by the *filterByExpr* function from the *edgeR*
562 package[61] in order to remove lowly expressed genes. DE was assessed with *DESeq2*[62]. FDR were
563 calculated using Benjamini-Hochberg correction[63].
564 Only the genes which passed the *filterByExpr* filtering were used for GSEA pathway analysis. GSEA was
565 performed with *fgsea* package[64] on a subset of pathways from the MSigDB's Hallmarks pathways[65]
566 (see SBM Table III). The $\log_2$Fold Change of the DE conditions compared with their matched UNTR
567 condition was used as an input of the analysis. Relative cell type enrichment was performed with
568 *xCell*[26] on a subset of cell types (SBM Table IV).

569

570 **Mass cytometry analysis**

571

572 Following 3 (T1) or 24 h (T2) of stimulation, samples from HD4-HD8 in all experimental conditions
573 were treated with Brefeldin A (BioLegend) (1:1,000) at 37°C for 4 h to favour intracellular cytokine
574 accumulation and were fixed with 1.6% of formaldehyde for 10 min at room temperature. Fixed
575 samples were stained with 0.05 µM Cell-ID™ Cisplatin-194-Pt (Fluidigm, South San Francisco, CA,
576 USA), a live-dead marker, for 1 min on a rocker. Samples for all experimental conditions from a given
577 donor and stimulation time point were then barcoded using the Cell-ID™ 20-Plex Pd Barcoding Kit
578 (Fluidigm) according to manufacturer's instructions. 12 samples were labelled concurrently in the
579 same tube following a three-step staining protocol. Briefly, 2.6-3.7 x 10^6 cells were firstly stained with
580 antibodies against surface markers (CD3, CD4, CD8a, CD62L, CD45RA, CD19, CD25, CD127, HLA-DR).
581 Following permeabilization with eBioscience™ Foxp3/Transcription Factor Staining Buffer Set
582 (Thermo Fisher Scientific) for 30 min at 4°C, cells were subsequently stained for the detection of
583 intracellular cytokines (IL-4, IL-5, IL-6, IL-23, IL-17A, IL-2, TNF-α, IFN-γ, GM-CSF, TGF-β, Granzyme B
584 and Perforin B) and cytoplasmic protein (RFP, used to detect mCherry expression). Cells were then
585 fixed in ice-cold 50% Methanol for 10 min at 4°C and underwent antibody staining for nuclear targets
586 (NFAT1 and FOXP3) and phosphoproteins (pSTAT4, pSTAT5, pp38, pERK1/2, pZAP70, pS6, pCREB and
587 pRB). Mass cytometry antibody details are listed in Supplementary Table 3. Stained cells were fixed
588 with 1.6% of formaldehyde for 10 min at room temperature on a rocker and incubated with Cell-ID™
589 Intercalator-Ir (Fluidigm) overnight at 4°C. The following day, experiments were performed on a Helios
590 mass cytometer (Fluidigm). EQ™ Four Element Calibration Beads (Fluidigm) were added to cell
591 suspensions immediately before acquisition to guarantee inter-sample comparability.
592
593 **Mass cytometry data pre-processing and analysis**
594
595 The resulting FCS files were normalised against EQ™ Four Element Calibration Beads, debarcoded and
596 uploaded on Cytobank platform. Viable single-cells were cleaned based on Gaussian parameters
597 (Event length, Centre, Offset and Residual), DNA content (193-Ir DNA) and Cisplatin (194-Pt) and gated
598 on CD19, CD3 and mCherry markers to detect B-cells, T-/CAR T-lymphocytes and CD19+ CAR T-cells.
599 Cell populations were exported from Cytobank and computationally analysed in Python (Python
600 version 3.7.6) or in R (R version 3.6.1) as described below.
601 Specifically, (EMD[19] and DREMI[45] scores were computed separately for each given stimulation
602 condition and time point between T-, CAR T-lymphocytes or CD19+ CAR T-cells and the entire cell
603 population as previously described[66] using CyGNAL repository (https://github.com/TAPE-
604 Lab/CyGNAL).

605 For the comparison between unstimulated and stimulated conditions, EMD scores were computed
606 separately for each given donor, culture condition (FMC63, CAT) and time point between CD3+ CAR
607 T-cells and the entire cell population within conditions.
608 The PCA performed on EMD scores of all 32 markers and the event counts in CD3+ T-cells from HD4-
609 HD8 across all the experimental conditions (Supplementary Fig. 3a, c-d) highlighted the lack of
610 activation of HD6 CAR T-cells upon antigen stimulation. For this reason, HD6 was excluded from the
611 analyses. PCA in Fig. 2d was generated on EMD scores of all 32 markers calculated on CD3+ T-cells
612 across all experimental conditions at T2. Heatmaps were generated using *pheatmap* package in R on
613 selected EMD (30 markers) scores or DREMI scores statistically different between the 2 CARs
614 normalised by row across specified experimental conditions.
615 Network analyses were performed using *tidygraph* and *ggraph* packages in R to compare signalling
616 connections in the two CAR constructs in specified experimental conditions. Nodes and edges were
617 coloured according to HD-averaged EMD and DREMI scores, respectively, which were computed on
618 CAR T-lymphocytes.
619 Additionally, pre-gated FCS files were imported in R, arcsinh transformed (cofactor = 5) and cell
620 clustered using the R packages *FlowSOM*[24] and *ConsensusClusterPlus*[67] as computed in[68]. The code for
621 the dimensional reduction analysis provided[68] was modified using R package *umap* for UMAP analysis.
622 UMAP analyses were performed downsampling at 1,000 cells and using default parameters.
623 Cytokine co-expression analysis was computed in R on CAR T (CD3+mCherry+) or trog+ CAR T
624 (CD3+mCherry+CD19+) pre-gated FCS files concatenated per donor for each given experimental
625 condition. An expression threshold of 1 was set for all the arcsinh transformed cytokine markers
626 except for TGF-ß, for which a threshold of 4 was selected. Chord diagrams of cytokine co-expression
627 were created with the R package *circlize*[69].
628 DNA staining intensity was assessed on unstimulated CAR T and on stimulated CD19- (CD19 expression
629 < 1) and CD19+ (CD19 expression >= 1) CAR T pre-gated FCS files arcsinh transformed.
630
631 **Statistical analyses**
632
633 Data are shown as mean ± standard error (se) and statistical analyses were performed in R or
634 GraphPad Prism 7 (GraphPad Software, LA Jolla, CA, USA) calculating Paired samples t-tests across
635 experimental conditions unless otherwise stated.
636 EMD, DREMI and polyfunctionality-related statistical analyses between selected experimental
637 conditions are reported in Supplementary Table 5.
638

639 **Data availability**

640

641 The RNA sequencing data and analyses are available at NCBI's Gene Expression Omnibus (GEO) data
642 repository with the accession code GSE157584 and in GitHub
643 (https://github.com/EduardoGCCM/CATvsFMC63_Michelozzi).
644 Mass cytometry raw and processed data will be made publicly available at
645 https://community.cytobank.org/.

646

647 **References**

648

649 1. Miliotou, A.N. & Papadopoulou, L.C. CAR T-cell Therapy: A New Era in Cancer Immunotherapy.
650 *Curr Pharm Biotechnol* **19**, 5-18 (2018).
651 2. Pehlivan, K.C., Duncan, B.B. & Lee, D.W. CAR-T Cell Therapy for Acute Lymphoblastic
652 Leukemia: Transforming the Treatment of Relapsed and Refractory Disease. *Curr Hematol*
653 *Malig Rep* **13**, 396-406 (2018).
654 3. Lee, D.W.*, et al.* Current concepts in the diagnosis and management of cytokine release
655 syndrome. *Blood* **124**, 188-195 (2014).
656 4. Gust, J.*, et al.* Endothelial Activation and Blood-Brain Barrier Disruption in Neurotoxicity after
657 Adoptive Immunotherapy with CD19 CAR-T Cells. *Cancer Discov* **7**, 1404-1419 (2017).
658 5. Watanabe, K., Kuramitsu, S., Posey, A.D., Jr. & June, C.H. Expanding the Therapeutic Window
659 for CAR T Cell Therapy in Solid Tumors: The Knowns and Unknowns of CAR T Cell Biology. *Front*
660 *Immunol* **9**, 2486 (2018).
661 6. Kowolik, C.M.*, et al.* CD28 costimulation provided through a CD19-specific chimeric antigen
662 receptor enhances in vivo persistence and antitumor efficacy of adoptively transferred T cells.
663 *Cancer Res* **66**, 10995-11004 (2006).
664 7. Singh, A.P.*, et al.* Development of a quantitative relationship between CAR-affinity, antigen
665 abundance, tumor cell depletion and CAR-T cell expansion using a multiscale systems PK-PD
666 model. *MAbs* **12**, 1688616 (2020).
667 8. Chmielewski, M., Hombach, A., Heuser, C., Adams, G.P. & Abken, H. T cell activation by
668 antibody-like immunoreceptors: increase in affinity of the single-chain fragment domain
669 above threshold does not increase T cell activation against antigen-positive target cells but
670 decreases selectivity. *J Immunol* **173**, 7647-7653 (2004).
671 9. Caruso, H.G.*, et al.* Tuning Sensitivity of CAR to EGFR Density Limits Recognition of Normal
672 Tissue While Maintaining Potent Antitumor Activity. *Cancer Res* **75**, 3505-3518 (2015).

673 10. Liu, X., *et al.* Affinity-Tuned ErbB2 or EGFR Chimeric Antigen Receptor T Cells Exhibit an
674 Increased Therapeutic Index against Tumors in Mice. *Cancer Res* **75**, 3596-3607 (2015).
675 11. Imai, C., *et al.* Chimeric receptors with 4-1BB signaling capacity provoke potent cytotoxicity
676 against acute lymphoblastic leukemia. *Leukemia* **18**, 676-684 (2004).
677 12. Ghorashian, S., *et al.* Enhanced CAR T cell expansion and prolonged persistence in pediatric
678 patients with ALL treated with a low-affinity CD19 CAR. *Nat Med* **25**, 1408-1414 (2019).
679 13. Ying, Z., *et al.* A safe and potent anti-CD19 CAR T cell therapy. *Nat Med* **25**, 947-953 (2019).
680 14. Valitutti, S., Muller, S., Cella, M., Padovan, E. & Lanzavecchia, A. Serial triggering of many T-
681 cell receptors by a few peptide-MHC complexes. *Nature* **375**, 148-151 (1995).
682 15. Caserta, S., Kleczkowska, J., Mondino, A. & Zamoyska, R. Reduced functional avidity promotes
683 central and effector memory CD4 T cell responses to tumor-associated antigens. *J Immunol*
684 **185**, 6545-6554 (2010).
685 16. Wang, X., *et al.* Phase 1 studies of central memory-derived CD19 CAR T-cell therapy following
686 autologous HSCT in patients with B-cell NHL. *Blood* **127**, 2980-2990 (2016).
687 17. Wang, X., *et al.* Comparison of naive and central memory derived CD8(+) effector cell
688 engraftment fitness and function following adoptive transfer. *Oncoimmunology* **5**, e1072671
689 (2016).
690 18. Turtle, C.J., *et al.* CD19 CAR-T cells of defined CD4+:CD8+ composition in adult B cell ALL
691 patients. *J Clin Invest* **126**, 2123-2138 (2016).
692 19. Orlova, D.Y., *et al.* Earth Mover's Distance (EMD): A True Metric for Comparing Biomarker
693 Expression Levels in Cell Populations. *PLoS One* **11**, e0151859 (2016).
694 20. Fuzzy Analysis (Program FANNY). in *Finding Groups in Data* 164-198 (1990).
695 21. Gomes-Silva, D., *et al.* Tonic 4-1BB Costimulation in Chimeric Antigen Receptors Impedes T
696 Cell Survival and Is Vector-Dependent. *Cell Rep* **21**, 17-26 (2017).
697 22. Frigault, M.J., *et al.* Identification of chimeric antigen receptors that mediate constitutive or
698 inducible proliferation of T cells. *Cancer Immunol Res* **3**, 356-367 (2015).
699 23. Long, A.H., *et al.* 4-1BB costimulation ameliorates T cell exhaustion induced by tonic signaling
700 of chimeric antigen receptors. *Nat Med* **21**, 581-590 (2015).
701 24. Van Gassen, S., *et al.* FlowSOM: Using self-organizing maps for visualization and interpretation
702 of cytometry data. *Cytometry A* **87**, 636-645 (2015).
703 25. Krummey, S.M., *et al.* CD45RB Status of CD8(+) T Cell Memory Defines T Cell Receptor Affinity
704 and Persistence. *Cell Rep* **30**, 1282-1291 e1285 (2020).
705 26. Aran, D., Hu, Z. & Butte, A.J. xCell: digitally portraying the tissue cellular heterogeneity
706 landscape. *Genome Biol* **18**, 220 (2017).

707 27. Allan, S.E.*, et al.* Activation-induced FOXP3 in human T effector cells does not suppress
708 proliferation or cytokine production. *Int Immunol* **19**, 345-354 (2007).
709 28. Ran, Q.*, et al.* CRIF1 interacting with CDK2 regulates bone marrow microenvironment-induced
710 G0/G1 arrest of leukemia cells. *PLoS One* **9**, e85328 (2014).
711 29. Carrette, F. & Surh, C.D. IL-7 signaling and CD127 receptor regulation in the control of T cell
712 homeostasis. *Semin Immunol* **24**, 209-217 (2012).
713 30. Kaech, S.M.*, et al.* Selective expression of the interleukin 7 receptor identifies effector CD8 T
714 cells that give rise to long-lived memory cells. *Nat Immunol* **4**, 1191-1198 (2003).
715 31. Holling, T.M., van der Stoep, N., Quinten, E. & van den Elsen, P.J. Activated human T cells
716 accomplish MHC class II expression through T cell-specific occupation of class II transactivator
717 promoter III. *J Immunol* **168**, 763-770 (2002).
718 32. Gourley, T.S. & Chang, C.H. Cutting edge: the class II transactivator prevents activation-
719 induced cell death by inhibiting Fas ligand gene expression. *J Immunol* **166**, 2917-2921 (2001).
720 33. Di Rosa, F.*, et al.* HLA class II molecules transduce accessory signals affecting the CD3 but not
721 the interleukin-2 activation pathway in T blasts. *Hum Immunol* **38**, 251-260 (1993).
722 34. Soroosh, P., Ine, S., Sugamura, K. & Ishii, N. OX40-OX40 ligand interaction through T cell-T cell
723 contact contributes to CD4 T cell longevity. *J Immunol* **176**, 5975-5987 (2006).
724 35. Sabatos, C.A.*, et al.* A synaptic basis for paracrine interleukin-2 signaling during homotypic T
725 cell interaction. *Immunity* **29**, 238-248 (2008).
726 36. Thurley, K., Gerecht, D., Friedmann, E. & Hofer, T. Three-Dimensional Gradients of Cytokine
727 Signaling between T Cells. *PLoS Comput Biol* **11**, e1004206 (2015).
728 37. Castellino, F.*, et al.* Chemokines enhance immunity by guiding naive CD8+ T cells to sites of
729 CD4+ T cell-dendritic cell interaction. *Nature* **440**, 890-895 (2006).
730 38. Hugues, S.*, et al.* Dynamic imaging of chemokine-dependent CD8+ T cell help for CD8+ T cell
731 responses. *Nat Immunol* **8**, 921-930 (2007).
732 39. Yiu, H.H., Graham, A.L. & Stengel, R.F. Dynamics of a cytokine storm. *PLoS One* **7**, e45027
733 (2012).
734 40. Betts, M.R.*, et al.* HIV nonprogressors preferentially maintain highly functional HIV-specific
735 CD8+ T cells. *Blood* **107**, 4781-4789 (2006).
736 41. Caccamo, N.*, et al.* Multifunctional CD4(+) T cells correlate with active Mycobacterium
737 tuberculosis infection. *Eur J Immunol* **40**, 2211-2220 (2010).
738 42. Rossi, J.*, et al.* Preinfusion polyfunctional anti-CD19 chimeric antigen receptor T cells are
739 associated with clinical outcomes in NHL. *Blood* **132**, 804-814 (2018).

740 43. Xhangolli, I.*, et al.* Single-cell Analysis of CAR-T Cell Activation Reveals A Mixed TH1/TH2
741 Response Independent of Differentiation. *Genomics Proteomics Bioinformatics* **17**, 129-139
742 (2019).
743 44. Frucht, D.M. IL-23: a cytokine that acts on memory T cells. *Sci STKE* **2002**, pe1 (2002).
744 45. Krishnaswamy, S.*, et al.* Systems biology. Conditional density-based analysis of T cell signaling
745 in single-cell data. *Science* **346**, 1250689 (2014).
746 46. Geginat, J., Sallusto, F. & Lanzavecchia, A. Cytokine-driven proliferation and differentiation of
747 human naive, central memory, and effector memory CD4(+) T cells. *J Exp Med* **194**, 1711-1719
748 (2001).
749 47. Li, C.*, et al.* Activation of p38 mitogen-activated protein kinase is critical step for acquisition
750 of effector function in cytokine-activated T cells, but acts as a negative regulator in T cells
751 activated through the T-cell receptor. *Immunology* **132**, 104-110 (2011).
752 48. Dodeller, F. & Schulze-Koops, H. The p38 mitogen-activated protein kinase signaling cascade
753 in CD4 T cells. *Arthritis Res Ther* **8**, 205 (2006).
754 49. Clark, A.R., Dean, J.L. & Saklatvala, J. Post-transcriptional regulation of gene expression by
755 mitogen-activated protein kinase p38. *FEBS Lett* **546**, 37-44 (2003).
756 50. Hamieh, M.*, et al.* CAR T cell trogocytosis and cooperative killing regulate tumour antigen
757 escape. *Nature* **568**, 112-116 (2019).
758 51. Rachmilewitz, J. & Lanzavecchia, A. A temporal and spatial summation model for T-cell
759 activation: signal integration and antigen decoding. *Trends Immunol* **23**, 592-595 (2002).
760 52. Weng, N.P., Araki, Y. & Subedi, K. The molecular basis of the memory T cell response:
761 differential gene expression and its epigenetic regulation. *Nat Rev Immunol* **12**, 306-315
762 (2012).
763 53. Sheih, A.*, et al.* Clonal kinetics and single-cell transcriptional profiling of CAR-T cells in patients
764 undergoing CD19 CAR-T immunotherapy. *Nat Commun* **11**, 219 (2020).
765 54. Ahmed, K.A., Munegowda, M.A., Xie, Y. & Xiang, J. Intercellular trogocytosis plays an
766 important role in modulation of immune responses. *Cell Mol Immunol* **5**, 261-269 (2008).
767 55. Osborne, D.G. & Wetzel, S.A. Trogocytosis results in sustained intracellular signaling in CD4(+)
768 T cells. *J Immunol* **189**, 4728-4739 (2012).
769 56. Andrews, S. FastQC: A quality control tool for high throughput sequence data. (2019).
770 57. Martin, M. Cutadapt removes adapter sequences from high-throughput sequencing reads.
771 *2011* **17**, 3 (2011).
772 58. Dobin, A.*, et al.* STAR: ultrafast universal RNA-seq aligner. *Bioinformatics* **29**, 15-21 (2013).

773 59. Frankish, A.*, et al.* GENCODE reference annotation for the human and mouse genomes.
774 *Nucleic Acids Research* **47**, D766-D773 (2018).
775 60. Liao, Y., Smyth, G.K. & Shi, W. featureCounts: an efficient general purpose program for
776 assigning sequence reads to genomic features. *Bioinformatics* **30**, 923-930 (2014).
777 61. Chen, Y., Lun, A. & Smyth, G. From reads to genes to pathways: differential expression analysis
778 of RNA-Seq experiments using Rsubread and the edgeR quasi-likelihood pipeline [version 2;
779 peer review: 5 approved]. *F1000Research* **5**(2016).
780 62. Love, M.I., Huber, W. & Anders, S. Moderated estimation of fold change and dispersion for
781 RNA-seq data with DESeq2. *Genome Biology* **15**, 550 (2014).
782 63. Benjamini, Y. & Hochberg, Y. Controlling the False Discovery Rate: A Practical and Powerful
783 Approach to Multiple Testing. *Journal of the Royal Statistical Society. Series B*
784 *(Methodological)* **57**, 289-300 (1995).
785 64. Korotkevich, G., Sukhov, V. & Sergushichev, A. Fast gene set enrichment analysis. *bioRxiv*,
786 060012 (2019).
787 65. Liberzon, A.*, et al.* The Molecular Signatures Database (MSigDB) hallmark gene set collection.
788 *Cell Syst* **1**, 417-425 (2015).
789 66. Qin, X.*, et al.* Cell-type-specific signaling networks in heterocellular organoids. *Nat Methods*
790 **17**, 335-342 (2020).
791 67. Wilkerson, M.D. & Hayes, D.N. ConsensusClusterPlus: a class discovery tool with confidence
792 assessments and item tracking. *Bioinformatics* **26**, 1572-1573 (2010).
793 68. Nowicka, M.*, et al.* CyTOF workflow: differential discovery in high-throughput high-
794 dimensional cytometry datasets. *F1000Res* **6**, 748 (2017).
795 69. Gu, Z., Gu, L., Eils, R., Schlesner, M. & Brors, B. circlize Implements and enhances circular
796 visualization in R. *Bioinformatics* **30**, 2811-2812 (2014).
797
798 **Acknowledgements**
799
800 We are grateful to Dr Ayad Eddaudi (UCL ICH Flow Cytometry facility) for support in cell-sorting. We
801 are grateful to Dr Thomas Adejumo (Fluidigm) for mass cytometry valuable suggestions and assistance
802 with protocols design. We thank Dr Anne Marijn Kramer (Amsterdam UMC) for generating CD19
803 FMC63 and CAT CAR transfer vector plasmids with S.G. and M.P. and P.J.A. We thank Mr Efstratios
804 Kirtsios (UCL) for useful discussion. The authors acknowledge the contribution of UCL Genomics
805 Facility. This work was supported by the NIHR GOSH BRC (NIHR GOSH BRC 17PA01), the views
806 expressed are those of the author(s) and not necessarily those of the NHS, the NIHR, or the

807 Department of Health. Part of this work was supported by the Leukaemia UK John Goldman Fellowship
808 to A.G. (2018/JGF/003), the Rosetrees Trust fund to A.G. (M700) and the Academy of Medical Sciences
809 Springboard Award to A.G. (SBF004\1025).
810

811 **Author contributions**

812

813 I.M.M. designed, performed and analyzed experiments, performed bioinformatic analyses of mass
814 cytometry experiments and contributed to writing the manuscript. E.G-C performed bioinformatic
815 analyses of transcriptomic data and wrote the relative bioinformatic supplementary information.
816 R.V.C.P. performed experiments and bioinformatic analyses of mass cytometry and transcriptomic
817 data. F.C-R provided data analysis tools and contributed to bioinformatic analyses of mass cytometry
818 experiments. P.P-C. performed transcriptomic bioinformatic analyses data checks and contributed to
819 writing the bioinformatic supplementary information. J. S., M.S., S.W.W and A.Gu. performed
820 experiments. S.G. and M.P. provided CAR constructs. C.J.T provided expertise in mass cytometry and
821 reagents. P.J.A. provided reagents and expertise and contributed to writing the manuscript. S.C.
822 supervised the bioinformatic analyses and contributed to writing the manuscript. A.G. designed and
823 supervised the project, performed and analyzed experiments and wrote the manuscript. All authors
824 provided critical feedback and helped shape the research, analysis and manuscript.
825

826 **Competing interests**

827

828 The authors declare no competing interests.

829 **Correspondence**

830

831 Corrispondente to Dr Alice Giustacchini.

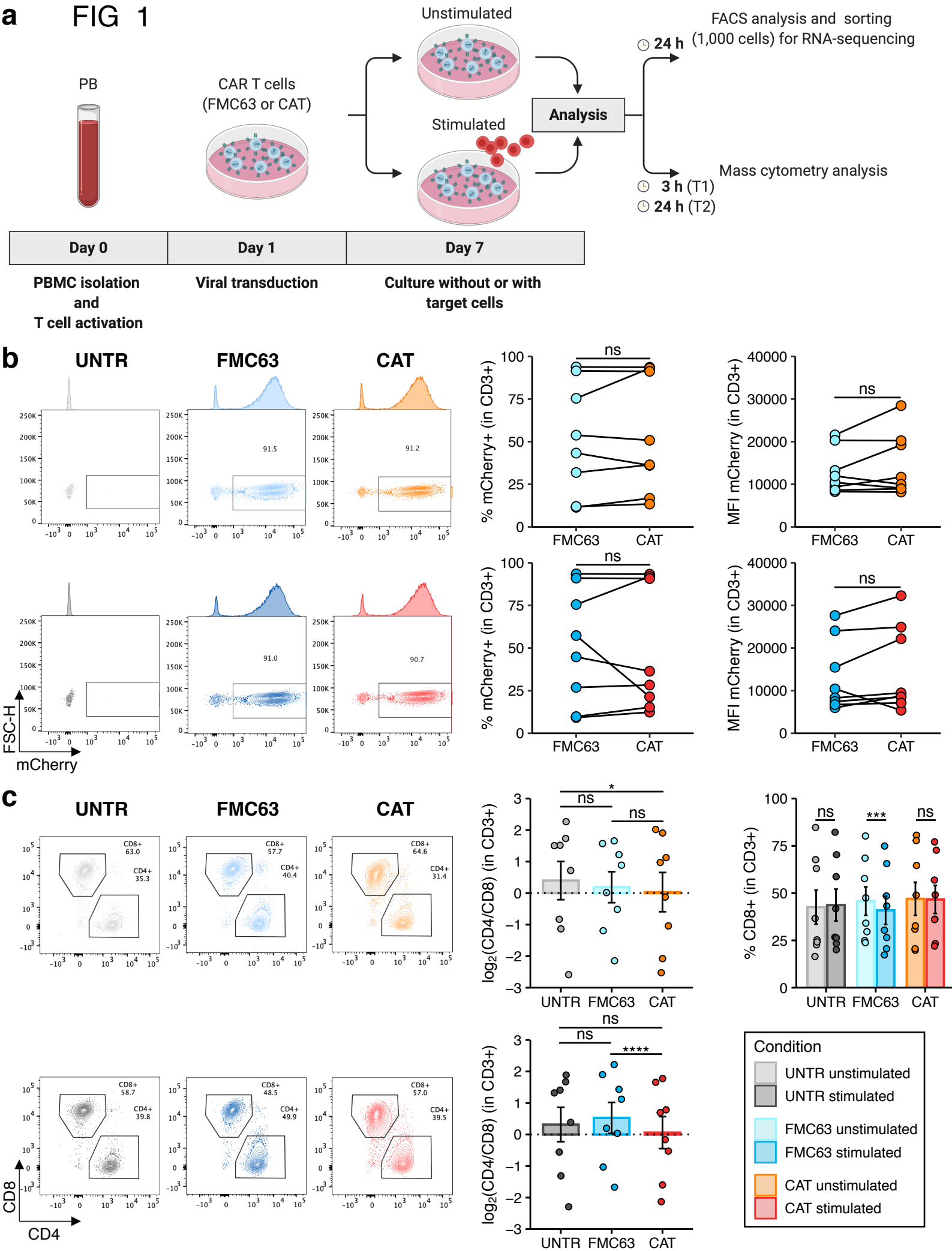
a
FIG 1
PB
CAR T cells
(FMC63 or CAT)
Unstimulated
Stimulated
Analysis
24 h
FACS analysis and sorting
(1,000 cells) for RNA-sequencing
3 h (T1)
24 h (T2)
Mass cytometry analysis
Day 0
Day 1
Day 7
PBMC isolation
and
T cell activation
Viral transduction
Culture without or with
target cells
b
UNTR
FMC63
CAT
91.5
91.2
91.0
90.7
FSC-H
mCherry
% mCherry+ (in CD3+)
MFI mCherry (in CD3+)
ns
FMC63
CAT
c
CD8+ 63.0
CD4+ 35.3
CD8+ 57.7
CD4+ 40.4
CD8+ 64.6
CD4+ 31.4
CD8+ 58.7
CD4+ 39.8
CD8+ 48.5
CD4+ 49.9
CD8+ 57.0
CD4+ 39.5
CD8
CD4
log2(CD4/CD8) (in CD3+)
% CD8+ (in CD3+)
UNTR
FMC63
CAT
*
***
****
Condition
UNTR unstimulated
UNTR stimulated
FMC63 unstimulated
FMC63 stimulated
CAT unstimulated
CAT stimulated

Fig. 1: Generation and phenotypic characterisation of CAR T-cells from HD-PBMCs.

a Experimental workflow. Peripheral Blood Mononuclear Cells (PBMCs) were isolated from HDs and LV transduced to express CD19 CAR construct (FMC63 or CAT) following overnight activation with CD3/CD28 beads.

Six days after transduction, CAR T-cells were cultured without (unstimulated) or with target cells (NALM6) at 1:1 ratio (stimulated). Unstimulated and stimulated cells were analysed by flow cytometry and sorted for RNA-sequencing 24 hours post-stimulation. Mass cytometry analysis was performed on unstimulated and stimulated cells at 3 h (T1) and 24 h (T2) post-stimulation.

Activated UNTR T-cells were used as a control throughout the experiment.

b (left) Representative FACS plots for mCherry expression in UNTR T-cells and FMC63 and CAT CAR T-cells at 7 days post-transduction. (middle) Spaghetti plots showing transduction levels of CAR T-cells as percentage of mCherry+ (in CD3+) and (right) as MFI of mCherry in transduced T-cells. Lines connect results from individual donors. Unstimulated (top) and stimulated conditions (bottom) are reported.

c (left) Representative FACS plots showing CD4 and CD8 composition of UNTR T-cells and FMC63 and CAT CAR T-cells. (middle) Variation ($\log_2$ fold change) of CD4 and CD8 proportion in UNTR T-cells and FMC63 and CAT CAR T-cells. The dotted horizontal line (0) represents the conditions in which CD4=CD8. Unstimulated (top) and stimulated conditions (bottom) are reported. (right) Percentage of CD8+ cells in unstimulated and stimulated UNTR T-cells and FMC63 and CAT CAR T-cells.

Data represent mean ± se.

b-c Statistical significance was calculated by Paired t-test. *$P < 0.05$, ***$P < 0.001$, ****$P < 0.0001$. n = 8 HDs, n = 2 independent experiments.

Each experimental condition is indicated by a specific colour code (Unstimulated conditions = UNTR light grey, FMC63 light blue, CAT orange; stimulated conditions = UNTR grey, FMC63 blue, CAT red).

FIG 2

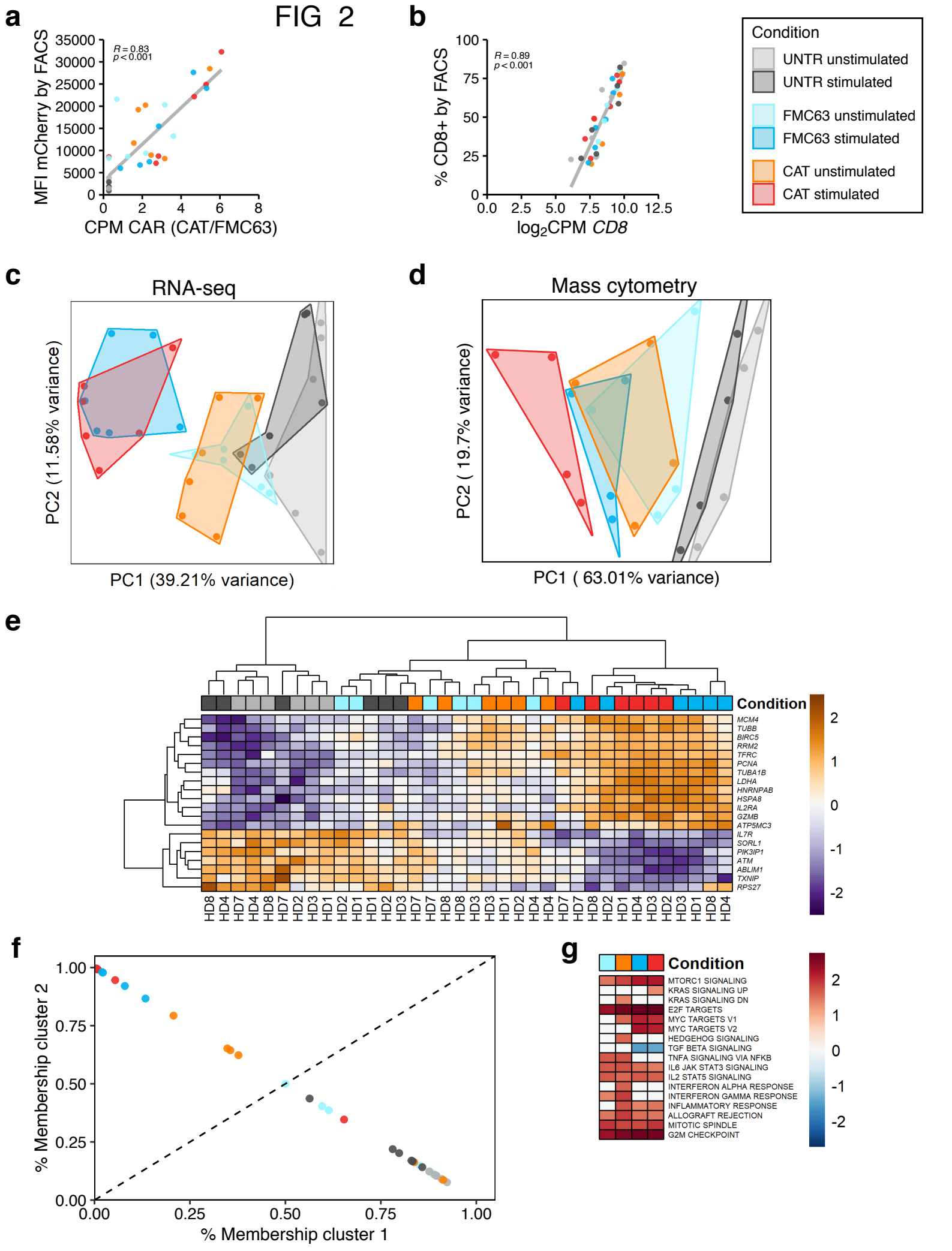
a
MFI mCherry by FACS
CPM CAR (CAT/FMC63)
R = 0.83
p < 0.001
b
% CD8+ by FACS
log2CPM CD8
R = 0.89
p < 0.001
Condition
UNTR unstimulated
UNTR stimulated
FMC63 unstimulated
FMC63 stimulated
CAT unstimulated
CAT stimulated
c
RNA-seq
PC2 (11.58% variance)
PC1 (39.21% variance)
d
Mass cytometry
PC2 (19.7% variance)
PC1 (63.01% variance)
e
Condition
MCM4
TUBB
BIRC5
RRM2
TFRC
PCNA
TUBA1B
LDHA
HNRNPAB
HSPA8
IL2RA
GZMB
ATP5MC3
IL7R
SORL1
PIK3IP1
ATM
ABLIM1
TXNIP
RPS27
f
% Membership cluster 2
% Membership cluster 1
g
Condition
MTORC1 SIGNALING
KRAS SIGNALING UP
KRAS SIGNALING DN
E2F TARGETS
MYC TARGETS V1
MYC TARGETS V2
HEDGEHOG SIGNALING
TGF BETA SIGNALING
TNFA SIGNALING VIA NFKB
IL6 JAK STAT3 SIGNALING
IL2 STAT5 SIGNALING
INTERFERON ALPHA RESPONSE
INTERFERON GAMMA RESPONSE
INFLAMMATORY RESPONSE
ALLOGRAFT REJECTION
MITOTIC SPINDLE
G2M CHECKPOINT

Fig. 2: RNA-seq and mass cytometry analyses of unstimulated and stimulated untransduced and CAR-transduced T-cells.

a Correlation of mCherry MFI measured by FACS with normalised RNA-seq counts (CPM) aligning to the scFv region of each of the two CARs (n = 6 HDs, n = 2 independent experiments). Pearson correlation and *P* values are displayed.

b Correlation of the percentage of CD8+ T-cells detected by FACS with *CD8* mRNA levels (n=6 HDs, n = 1 independent experiment). Pearson correlation and *P* values are displayed.

c PCA of the top 500 variable genes from RNA-seq analysis across all the experimental conditions (n = 6 HDs, n = 2 independent experiments).

d PCA of mass cytometry EMD scores computed at T2 (24 h stimulation) in CD3+ cells across all the experimental conditions (n = 4 HDs, n = 1 independent experiment).

e Heatmap showing the hierarchical clustering of all the experimental conditions analysed displaying the top 20 variable genes from RNA-seq PC1 (n = 6 HDs, n = 2 independent experiments).

f Fuzzy clustering analysis of RNA-seq data across all experimental conditions (n = 6 HDs, n = 2 independent experiments).

g GSEA of HALLMARK gene sets for (1) FMC63 or (2) CAT CAR T unstimulated condition *vs* UNTR unstimulated cells, (3) FMC63 or (4) CAT CAR T stimulated condition *vs* UNTR stimulated cells (n = 6 HDs, n = 2 independent experiments). Non-significant enrichment scores were set to zero. Gene sets with no significant enrichment scores are not shown.

a-g Each experimental condition is indicated by a specific colour code (Unstimulated conditions = UNTR light grey, FMC63 light blue, CAT orange; stimulated conditions = UNTR grey, FMC63 blue, CAT red).

FIG 3

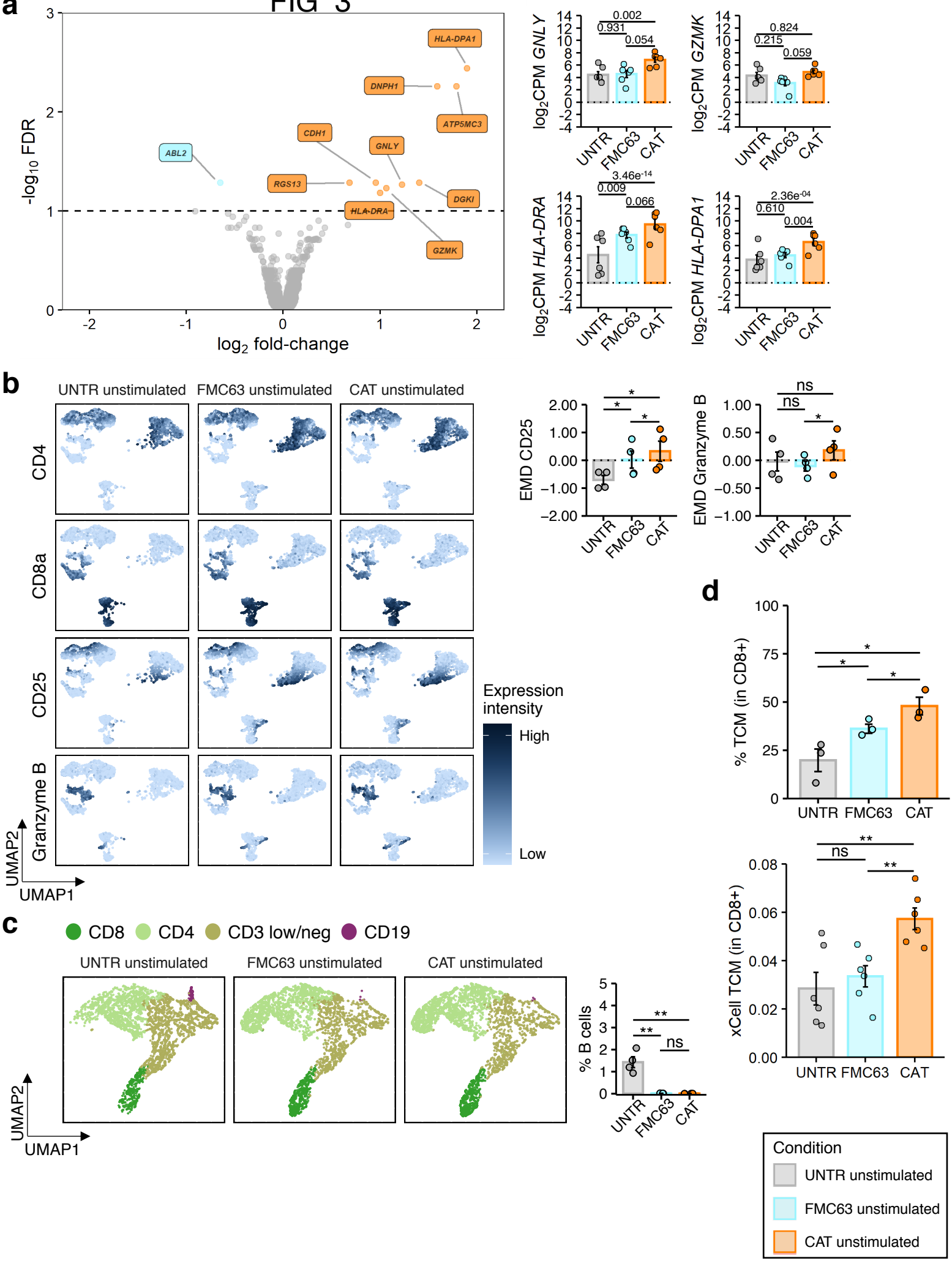
a
-log10 FDR
log2 fold-change
HLA-DPA1
DNPH1
ATP5MC3
CDH1
GNLY
ABL2
RGS13
DGKI
HLA-DRA
GZMK
log2CPM GNLY
0.002
0.931
0.054
log2CPM GZMK
0.824
0.215
0.059
log2CPM HLA-DRA
3.46e-14
0.009
0.066
log2CPM HLA-DPA1
2.36e-04
0.610
0.004
UNTR
FMC63
CAT
b
UNTR unstimulated
FMC63 unstimulated
CAT unstimulated
CD4
CD8a
CD25
Granzyme B
UMAP2
UMAP1
Expression intensity
High
Low
EMD CD25
EMD Granzyme B
ns
c
CD8
CD4
CD3 low/neg
CD19
% B cells
d
% TCM (in CD8+)
xCell TCM (in CD8+)
Condition
UNTR unstimulated
FMC63 unstimulated
CAT unstimulated

Fig. 3: Molecular characterisation of unstimulated CAR-transduced T-cells.

a (left) Volcano plot showing DE genes between unstimulated FMC63 and CAT CAR T-cells. The dashed horizontal line represents the statistical significance threshold (FDR < 0.1). (right) The barplots show the expression of selected DE genes (FDR < 0.1) in unstimulated untransduced and transduced T-cells (n = 6 HDs, n = 2 independent experiments).

b (left) UMAP showing the expression of selected markers (CD4, CD8a, CD25, Granzyme B) detected by mass cytometry at T2 (24 h stimulation) in unstimulated CD3+ cells across all the experimental conditions. The colour of the scale reflects the protein expression levels.

(right) The barplots show the expression of mass cytometry EMD scores for CD25 and Granzyme B in unstimulated CD3+ cells across all the experimental conditions at T2. The dotted horizontal line (0) represents the average expression of a specific marker across all the experimental conditions analysed. (n = 4 HDs, n = 1 independent experiment).

c (left) UMAP representation of the 4 cell populations (CD8, CD4, CD3 low/neg, CD19) identified by FlowSOM analysis in unstimulated samples analysed by mass cytometry at T2 (24 h stimulation). The cell types are indicated by different colours. (right) Percentage of residual B-cells detected by mass cytometry in unstimulated samples at T2. (n = 4 HDs, n = 1 independent experiment).

d (top) Barplot showing the percentage of T_{CM} (CD45RA-CD62L+) in unstimulated CD8+ UNTR T-cells and FMC63 and CAT CAR T-cells (n = 3 HDs, n = 1 independent experiment) measured by FACS. (bottom) xCell score inferring the enrichment of CD8 T_{CM} in bulk RNA-seq results from unstimulated UNTR (CD3+) T-cells and FMC63 and CAT (CD3+mCherry+) CAR T-cells (n = 6 HDs, n = 2 independent experiments).

a-d Barplots show mean ± se. Statistical significance was calculated by Paired t-test. *P < 0.05, **P < 0.01. Each experimental condition is indicated by a specific colour code (UNTR light grey, FMC63 light blue, CAT orange).

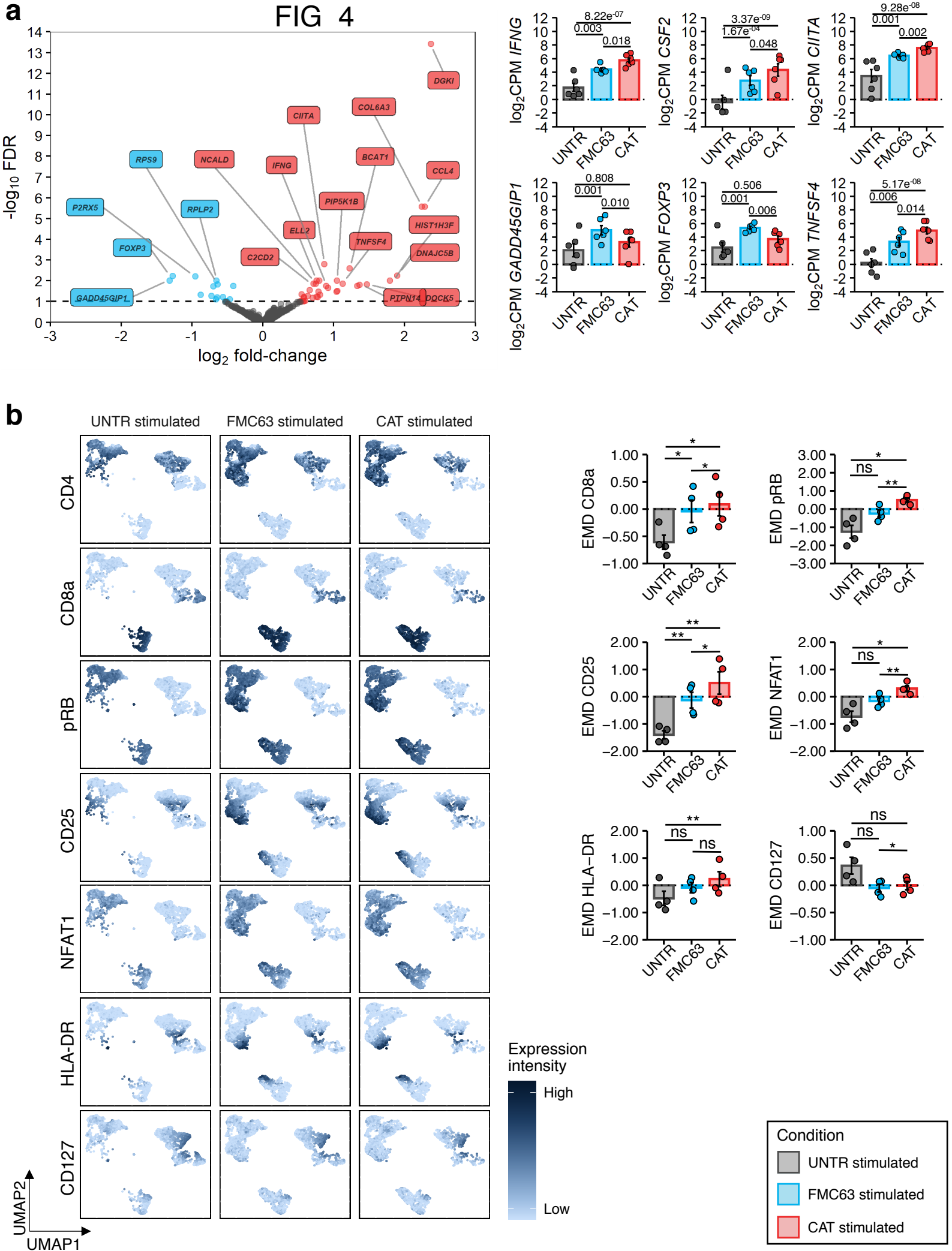
FIG 4
a
-log10 FDR
log2 fold-change
DGKI
COL6A3
CIITA
RPS9
NCALD
IFNG
BCAT1
CCL4
P2RX5
RPLP2
PIP5K1B
HIST1H3F
ELL2
FOXP3
TNFSF4
C2CD2
DNAJC5B
GADD45GIP1
PTPN14
DOCK5
log2CPM IFNG
log2CPM CSF2
log2CPM CIITA
log2CPM GADD45GIP1
log2CPM FOXP3
log2CPM TNFSF4
8.22e-07
0.003
0.018
3.37e-09
1.67e-04
0.048
9.28e-08
0.001
0.002
0.808
0.001
0.010
0.506
0.001
0.006
5.17e-08
0.006
0.014
UNTR
FMC63
CAT
b
UNTR stimulated
FMC63 stimulated
CAT stimulated
CD4
CD8a
pRB
CD25
NFAT1
HLA-DR
CD127
UMAP2
UMAP1
Expression intensity
High
Low
EMD CD8a
EMD pRB
EMD CD25
EMD NFAT1
EMD HLA-DR
EMD CD127
ns
Condition
UNTR stimulated
FMC63 stimulated
CAT stimulated

Fig. 4: Molecular characterisation of stimulated CAR-transduced T-cells.

a (left) Volcano plot showing DE genes between FMC63 and CAT CAR T-cells upon NALM6 co-culture. The dashed horizontal line represents the statistical significance threshold (FDR < 0.1). (right) The barplots show the expression of selected DE genes (FDR < 0.1) in stimulated UNTR T-cells and in CAR T-cells (n = 6 HDs, n = 2 independent experiments).

b (left) UMAP showing the expression of selected markers (CD4, CD8a, pRB, CD25, NFAT1, HLA-DR, CD127) detected by mass cytometry at T2 (24 h stimulation) in stimulated CD3+ cells across all the experimental conditions (UNTR, FMC63, CAT). The colour of the scale reflects the protein expression levels.

(right) The barplots show the expression of mass cytometry EMD scores for CD8a, pRB, CD25, NFAT1, HLA-DR and CD127 in stimulated CD3+ cells across all the experimental conditions at T2 (24 h stimulation). The dotted horizontal line (0) represents the average expression of a specific marker across all the experimental conditions analysed. (n = 4 HDs, n = 1 independent experiment). Statistical significance was calculated by Paired t-test. *P < 0.05, **P < 0.01.

a-b Barplots show mean ± se. Each experimental condition is indicated by a specific colour code (UNTR grey, FMC63 blue, CAT red).

FIG 5

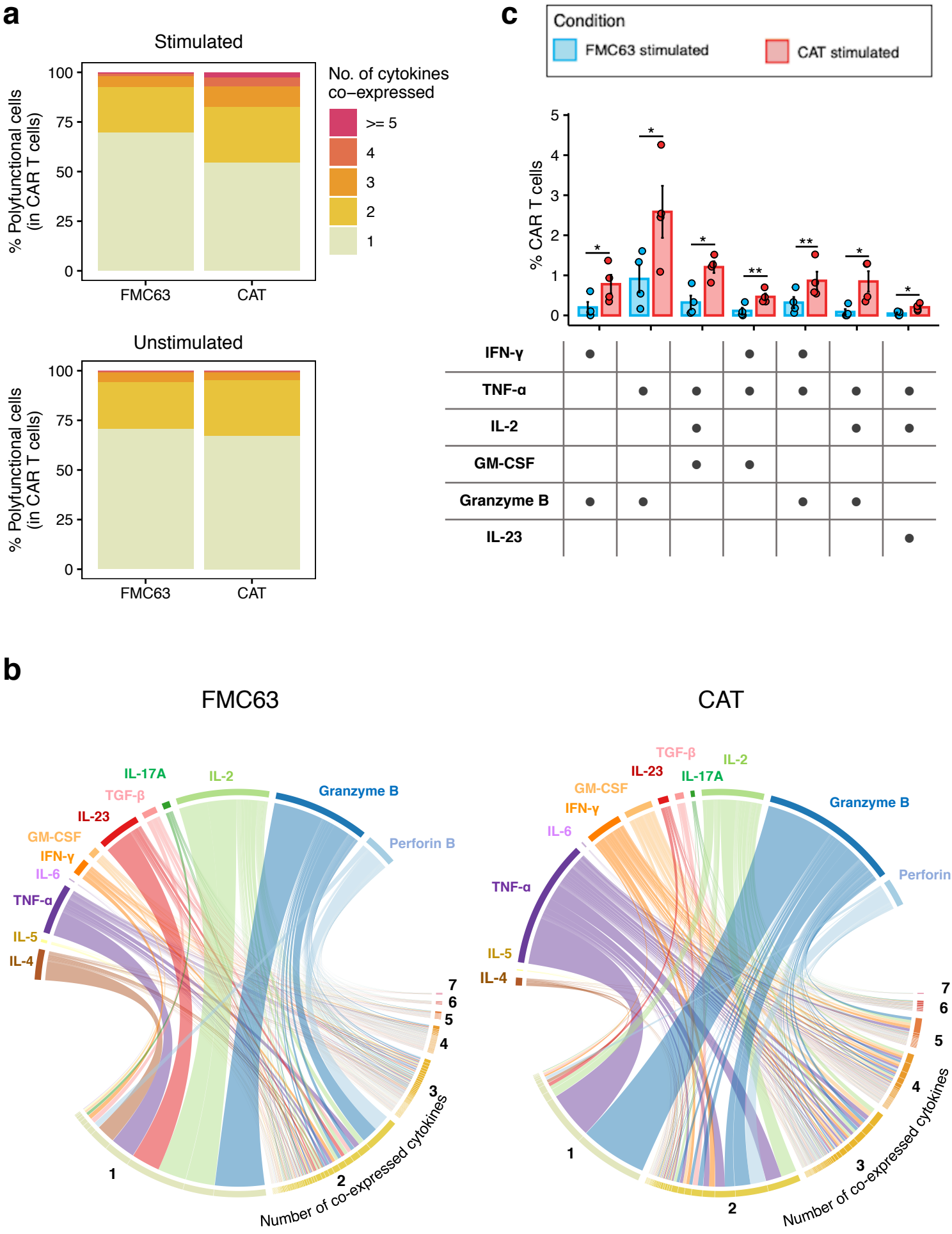
a
Stimulated
% Polyfunctional cells (in CAR T cells)
100
75
50
25
0
FMC63
CAT
No. of cytokines co−expressed
>= 5
4
3
2
1
Unstimulated
% Polyfunctional cells (in CAR T cells)
100
75
50
25
0
FMC63
CAT
c
Condition
FMC63 stimulated
CAT stimulated
% CAR T cells
5
4
3
2
1
0
*
*
*
**
**
*
*
IFN-γ
TNF-α
IL-2
GM-CSF
Granzyme B
IL-23
b
FMC63
IL-17A
IL-2
Granzyme B
TGF-β
IL-23
GM-CSF
IFN-γ
IL-6
TNF-α
IL-5
IL-4
Perforin B
7
6
5
4
3
2
1
Number of co-expressed cytokines
CAT
TGF-β
IL-2
IL-23
IL-17A
GM-CSF
IFN-γ
IL-6
TNF-α
IL-5
IL-4
Granzyme B
Perforin B
7
6
5
4
3
2
1
Number of co-expressed cytokines

Fig. 5: Cytokine polyfunctionality in CAR-transduced T-cells at 3 h post-stimulation.

a The stacked barplots show the percentage of stimulated (top) and unstimulated (bottom) CAR T-cells (CD3+mCherry+) expressing 1 to 4 or >=5 cytokines/cell at T1 (3 h stimulation) as measured by mass cytometry.

b The circos plots show all the combinations of the 12 cytokines analysed in stimulated FMC63 (left) and CAT (right) CAR T-cells at T1 (3 h stimulation) by mass cytometry. The numbers indicate patterns of cytokine co-expression (from 1 to 7 cytokines/cell). A specific colour code has been assigned to each cytokine.

c The barplots show the percentage of the statistically significant combinations of cytokines co-expressed in stimulated FMC63 and CAT CAR T-cells at T1 (3 h stimulation) by mass cytometry. Data represent mean ± se. Statistical significance was calculated by Paired t-test. $*P < 0.05$, $**P < 0.01$. Each experimental condition is indicated by a specific colour code (FMC63 = blue, CAT = red).

a-c n = 4 HDs, n = 1 independent experiment.

FIG 6

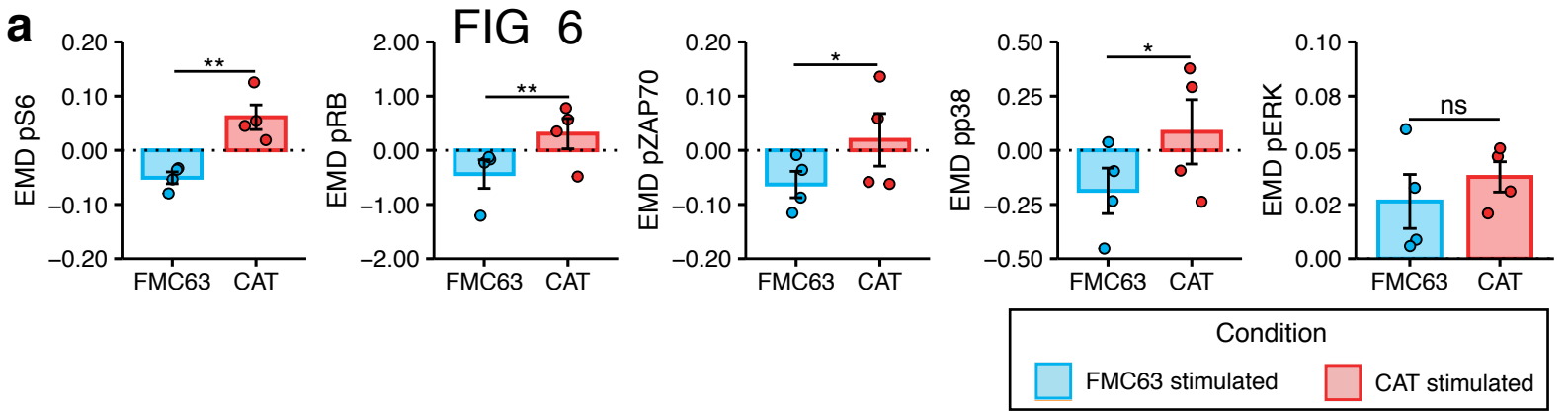
a
EMD pS6
EMD pRB
EMD pZAP70
EMD pp38
EMD pERK
FMC63
CAT
**
**
*
*
ns
Condition
FMC63 stimulated
CAT stimulated

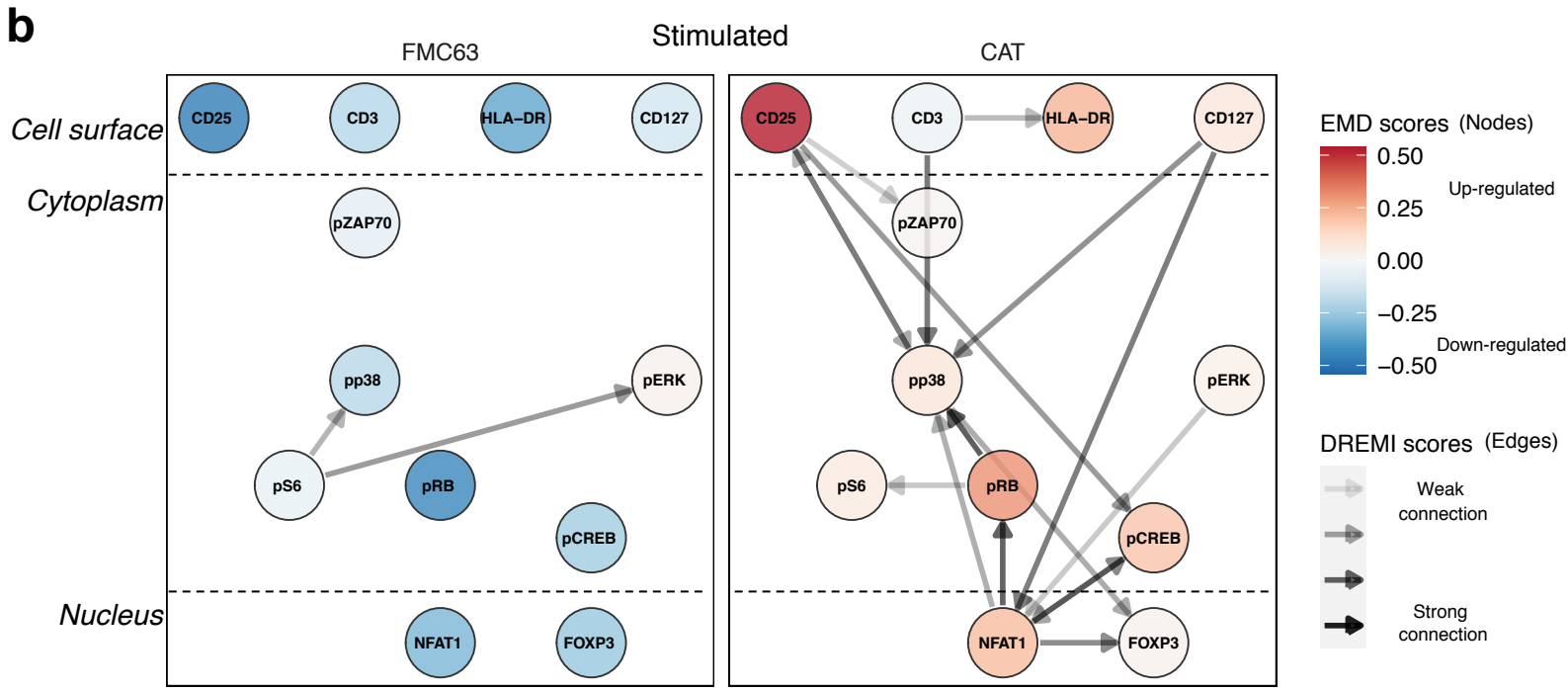
b
Stimulated
FMC63
CAT
Cell surface
Cytoplasm
Nucleus
CD25
CD3
HLA–DR
CD127
pZAP70
pp38
pERK
pS6
pRB
pCREB
NFAT1
FOXP3
EMD scores (Nodes)
0.50
0.25
0.00
−0.25
−0.50
Up-regulated
Down-regulated
DREMI scores (Edges)
Weak connection
Strong connection

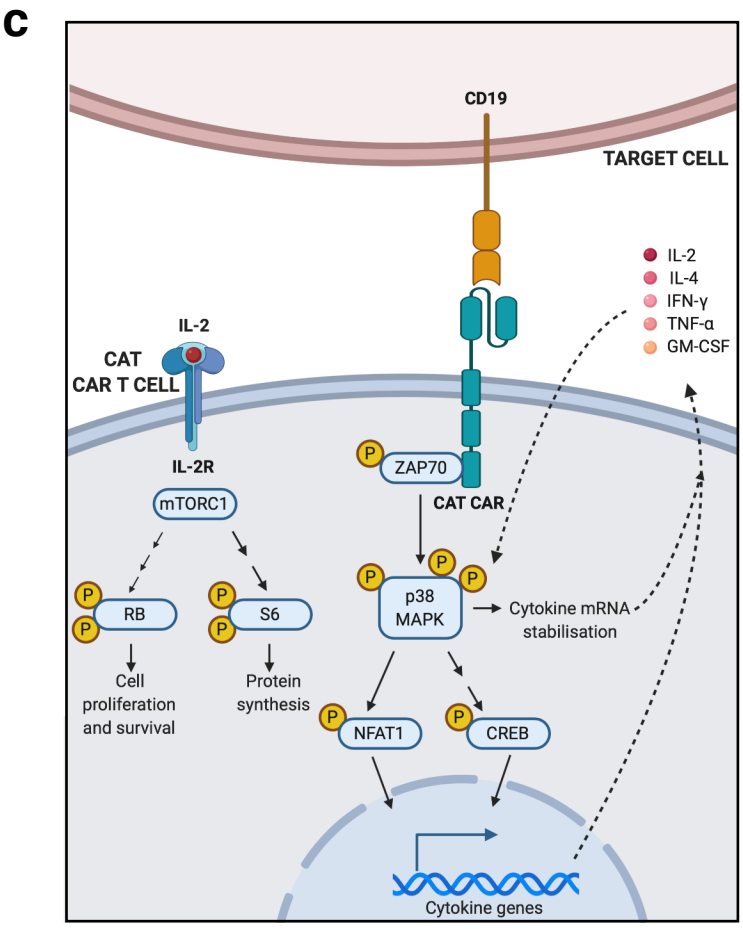
c
CD19
TARGET CELL
IL-2
IL-4
IFN-γ
TNF-α
GM-CSF
IL-2
CAT
CAR T CELL
IL-2R
mTORC1
ZAP70
CAT CAR
RB
S6
p38
MAPK
Cytokine mRNA
stabilisation
Cell
proliferation
and survival
Protein
synthesis
NFAT1
CREB
Cytokine genes

Fig. 6: Intracellular signalling analyses in CAR-transduced T-cells at 24 h post-stimulation

a The barplots show the expression of mass cytometry EMD scores for selected phosphoproteins (pS6, pRB, pZAP70, pp38, pERK) in stimulated FMC63 and CAT CAR T-cells at T2 (24 h stimulation). The dotted horizontal line (0) represents the average expression of a specific marker across all the experimental conditions analysed. Barplots show mean ± se (n = 4 HDs, n = 1 independent experiment). Statistical significance was calculated by Paired t-test. $*P < 0.05$, $**P < 0.01$. Each experimental condition is indicated by a specific colour code (FMC63 blue, CAT red).

b Differential signalling network in stimulated FMC63 (left) and CAT (right) CAR T-cells at T2 (24 h stimulation) post-stimulation. The nodes are coloured by HD-averaged EMD scores computed between stimulated CAR T-cells at T2 and arrows, whose transparency reflects HD-averaged DREMI scores, indicate differential markers connectivity between the two CAR products ($P <= 0.05$, n = 4 HDs, n = 1 independent experiment).

c Schematized model of the proposed intracellular signalling occurring preferentially in activated CAT as compared to FMC63 CAR T-cells upon CD19+ target cell engagement. Stimulated CAT CAR T-cells show sustained activation of mTORC1 pathway with consequent elevated protein synthesis and cellular proliferation and survival (pS6 and pRB). Moreover, p38 MAPK cascade, initiated by the CAR CD3ζ chain through pZAP70, results in cytokine genes transcription (probably mediated by NFAT1 and pCREB) and mRNA stabilisation. The expressed cytokines (including IL-2, IL-4, TNF-α, IFN-γ, GM-CSF) could in turn sustain CAT CAR T-cell activation in an antigen independent manner.

FIG 7

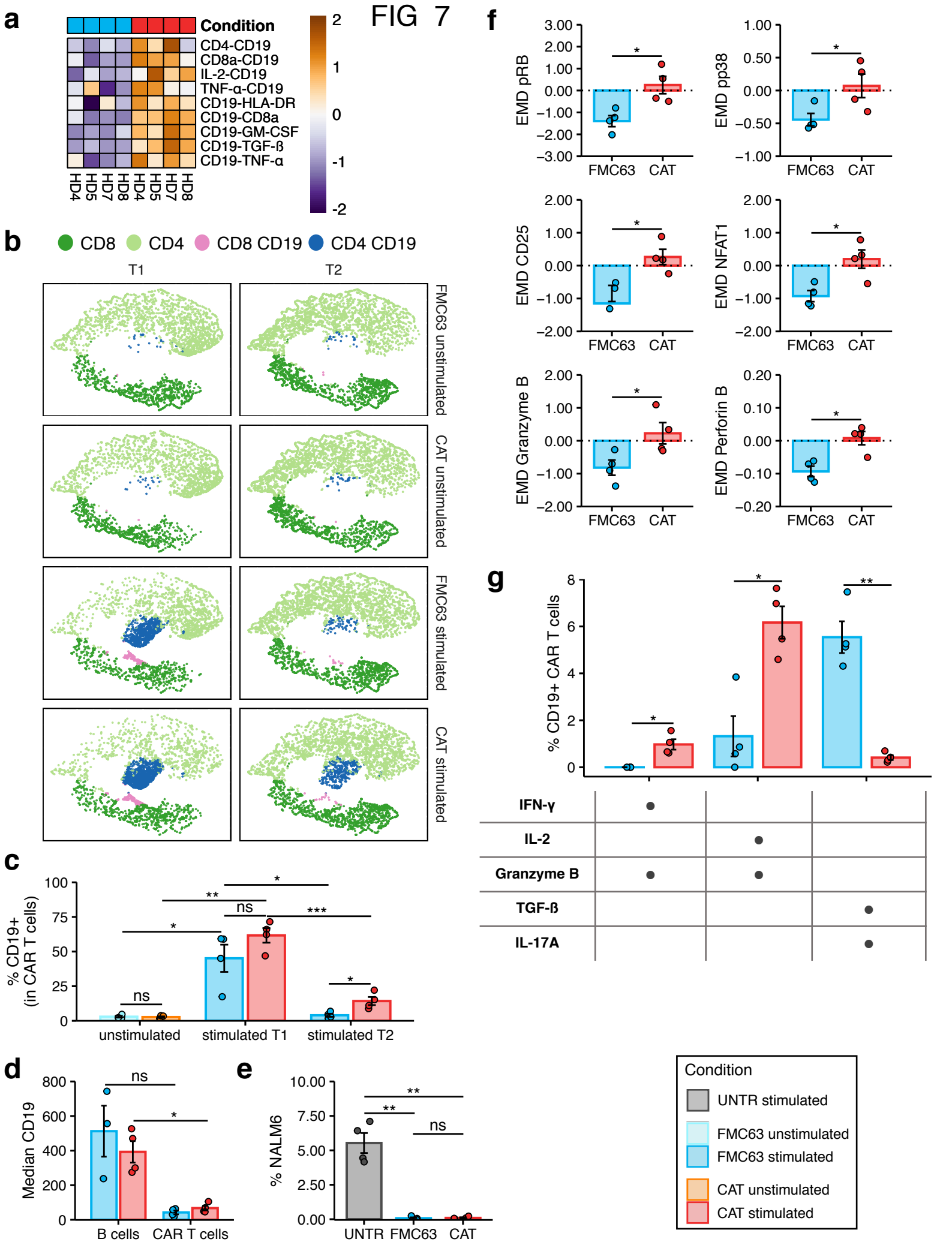
a
Condition
CD4-CD19
CD8a-CD19
IL-2-CD19
TNF-α-CD19
CD19-HLA-DR
CD19-CD8a
CD19-GM-CSF
CD19-TGF-ß
CD19-TNF-α
HD4
HD5
HD7
HD8
HD4
HD5
HD7
HD8
2
1
0
-1
-2
b
CD8
CD4
CD8 CD19
CD4 CD19
T1
T2
FMC63 unstimulated
CAT unstimulated
FMC63 stimulated
CAT stimulated
c
% CD19+ (in CAR T cells)
unstimulated
stimulated T1
stimulated T2
ns
d
Median CD19
B cells
CAR T cells
e
% NALM6
UNTR
FMC63
CAT
f
EMD pRB
EMD pp38
EMD CD25
EMD NFAT1
EMD Granzyme B
EMD Perforin B
FMC63
CAT
g
% CD19+ CAR T cells
IFN-γ
IL-2
Granzyme B
TGF-ß
IL-17A
Condition
UNTR stimulated
FMC63 unstimulated
FMC63 stimulated
CAT unstimulated
CAT stimulated

Fig. 7: Molecular characterisation of trogocytic CAR-transduced T-cells.

a Heatmap showing CD19 related-mass cytometry DREMI scores computed at T1 (3 h stimulation) in CD3+ CAR T-cells across all the stimulated experimental conditions.

b UMAP representation across experimental conditions of the changes in proportion of 4 cell populations (CD8, CD4, CD8 CD19, CD4 CD19) identified by FlowSOM analysis in CAR T-cells analysed by mass cytometry at T1 (3 h stimulation) and T2 (24 h stimulation). The CAR T-cell subtypes are indicated by different colours. (n = 4 HDs, n = 1 independent experiment).

c Percentage of trog+ CAR T-cells detected by mass cytometry in unstimulated (at T2, 24 h stimulation) and in stimulated transduced samples (at T1 and T2).

d Median intensity of CD19 expression in B-cells and in trog+ CAR T-cells from stimulated CAR-transduced samples at T1 (3 h stimulation) by mass cytometry. Statistical significance was calculated by Mann-Withney test. *$P < 0.05$.

e Percentage of residual NALM6 cells detected by mass cytometry in stimulated samples at T2 (24 h stimulation).

f The barplots show the expression of mass cytometry EMD scores for pRB, pp38, CD25, NFAT1, Granzyme B and Perforin B in stimulated trog+ CAR T-cells at T2 (24 h stimulation). The dotted horizontal line (0) represents the average expression of a specific marker across all the experimental conditions analysed.

g The barplots show the percentage of the statistically different combinations of cytokines co-expressed in stimulated trog+ FMC63 and CAT CAR T-cells at T2 (24 h stimulation) by mass cytometry.

a, c, e-g Statistical significance was calculated by Paired t-test. *$P < 0.05$, **$P<0.01$, ***$P<0.001$.

a, c-g Data represent mean ± se (n = 4 HDs, n = 1 independent experiment). Each experimental condition is indicated by a specific colour code (Unstimulated conditions = FMC63 light blue, CAT orange; stimulated conditions = UNTR grey, FMC63 blue, CAT red).

Suppl FIG 1

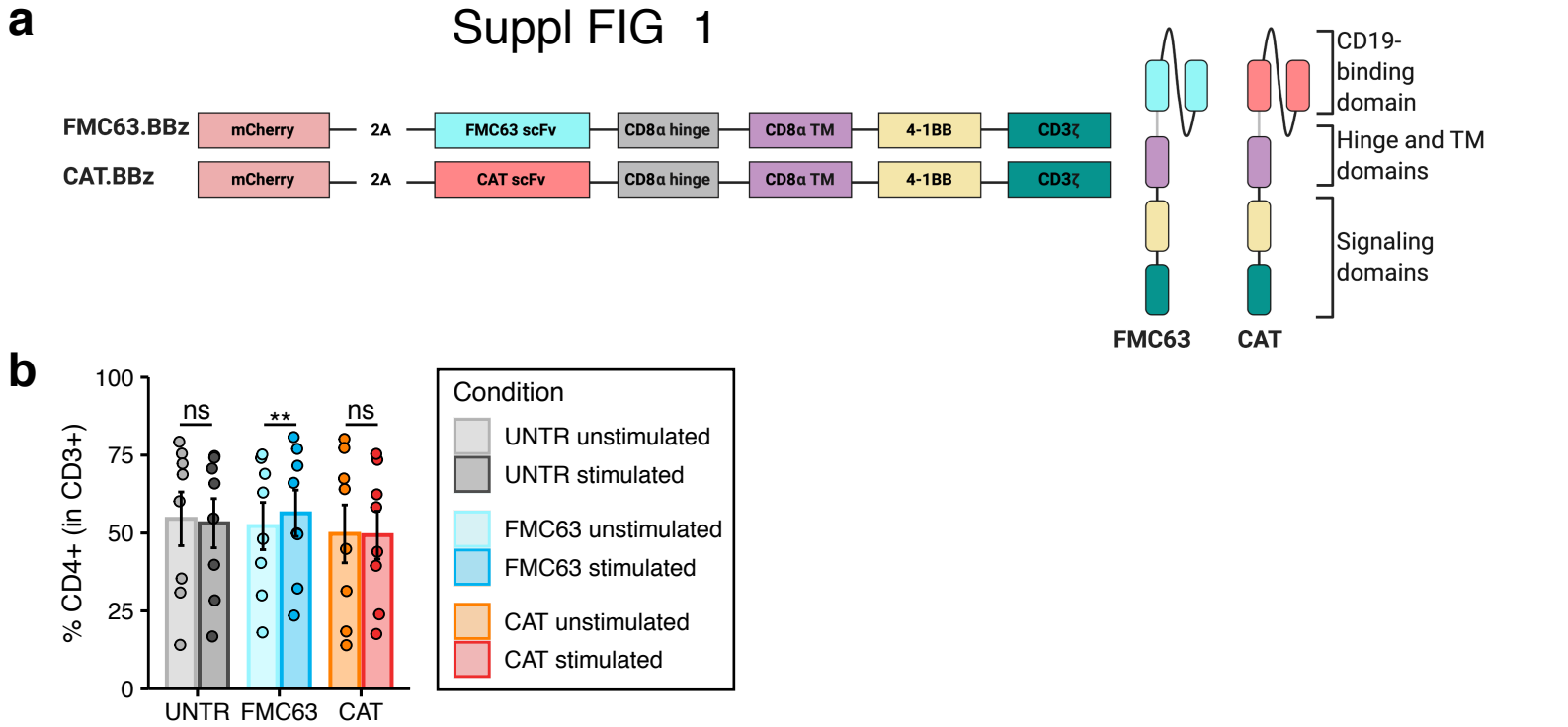
a
FMC63.BBz
mCherry
2A
FMC63 scFv
CD8α hinge
CD8α TM
4-1BB
CD3ζ
CAT.BBz
mCherry
2A
CAT scFv
CD8α hinge
CD8α TM
4-1BB
CD3ζ
CD19-binding domain
Hinge and TM domains
Signaling domains
FMC63
CAT
b
% CD4+ (in CD3+)
100
75
50
25
0
ns
**
ns
UNTR
FMC63
CAT
Condition
UNTR unstimulated
UNTR stimulated
FMC63 unstimulated
FMC63 stimulated
CAT unstimulated
CAT stimulated

Supplementary Fig. 1: Generation and phenotypic characterisation of CAR T-cells from HD-PBMCs.

a (left) Schematic representation of the FMC63 and CAT bicistronic lentiviral vector constructs and (right) of FMC63 and CAT CAR structure. Both constructs are second generation CARs composed by an anti-CD19 scFv, derived from FMC63 or CAT13.1E10 hybridoma, a CD8α hinge, a CD8α transmembrane domain (TM), a 4-1BB costimulatory domain and a CD3ζ signalling domain linked to a reporter gene (mCherry), marker of transduction.

b The bar graph shows the percentage of CD4+ cells in unstimulated and stimulated UNTR T-cells and FMC63 and CAT CAR T-cells. Each experimental condition is indicated by a specific colour code (Unstimulated conditions = UNTR light grey, FMC63 light blue, CAT orange; stimulated conditions = UNTR grey, FMC63 blue, CAT red). Data represent mean ± se. Statistical significance was calculated by Paired t-test. $^{**}P < 0.01$. n = 8 HDs, n = 2 independent experiments.

Suppl FIG 2

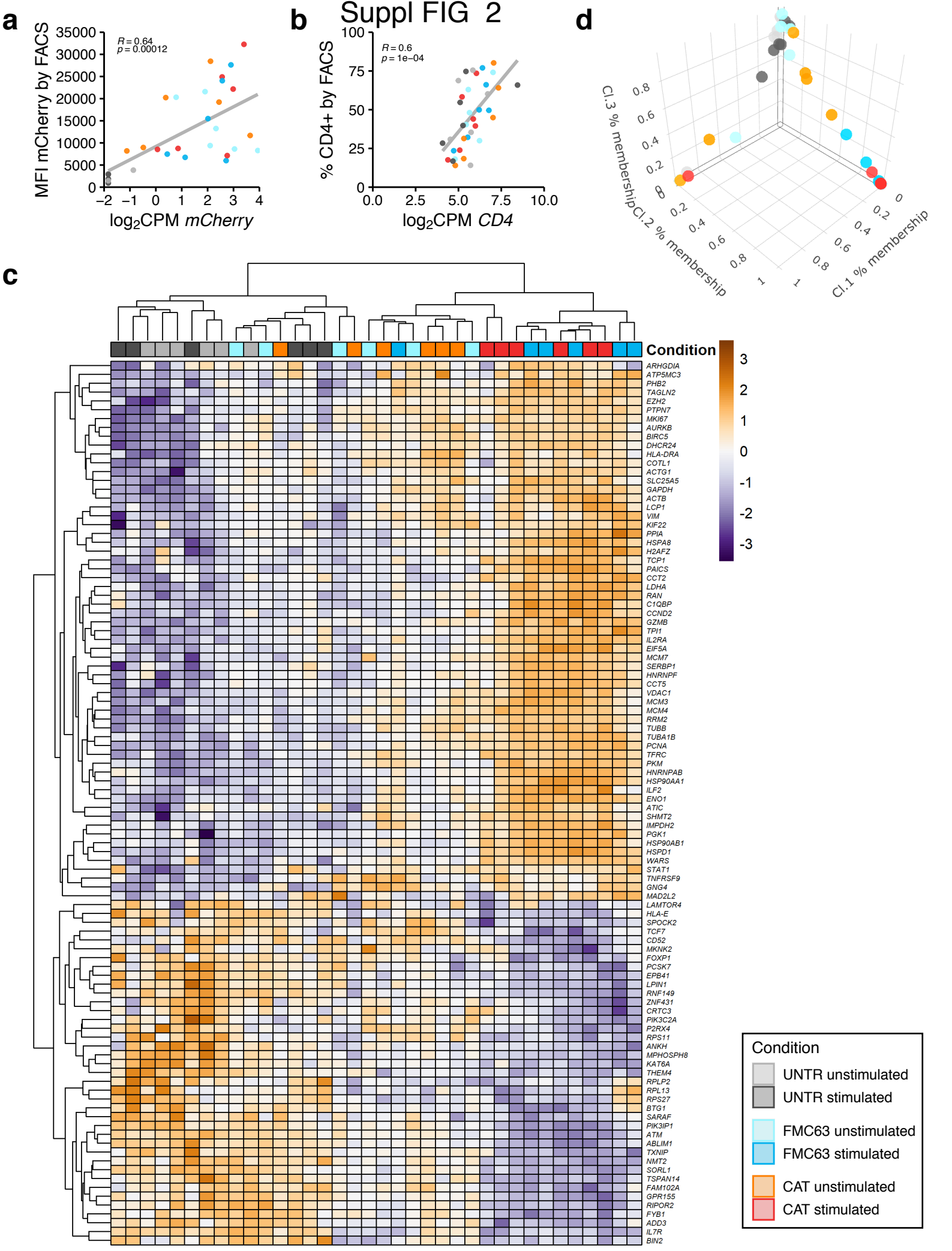
a
MFI mCherry by FACS
log2CPM mCherry
R = 0.64
p = 0.00012
b
% CD4+ by FACS
log2CPM CD4
R = 0.6
p = 1e−04
d
Cl.3 % membership
Cl.2 % membership
Cl.1 % membership
c
Condition
UNTR unstimulated
UNTR stimulated
FMC63 unstimulated
FMC63 stimulated
CAT unstimulated
CAT stimulated

Supplementary Fig. 2: RNA-seq analyses of unstimulated and stimulated untransduced and CAR-transduced T-cells.

a Correlation of mCherry MFI measured by FACS with *mCherry* mRNA levels (n = 6 HDs, n = 2 independent experiments). Pearson correlation and *P* values are displayed.

b Correlation of the percentage of CD4+ T-cells detected by FACS with *CD4* mRNA levels (n = 6 HDs, n = 2 independent experiments). Pearson correlation and *P* values are displayed.

c Heatmap showing the hierarchical clustering of all the experimental conditions analysed displaying the top 100 variable genes from RNA-seq PC1 (n = 6 HDs, n = 2 independent experiments).

d 3D fuzzy clustering analysis of RNA-seq data across all experimental conditions (n = 6 HDs, n = 2 independent experiments).

a-d Each experimental condition is indicated by a specific colour code (Unstimulated conditions = UNTR light grey, FMC63 light blue, CAT orange; stimulated conditions = UNTR grey, FMC63 blue, CAT red).

Suppl FIG 3

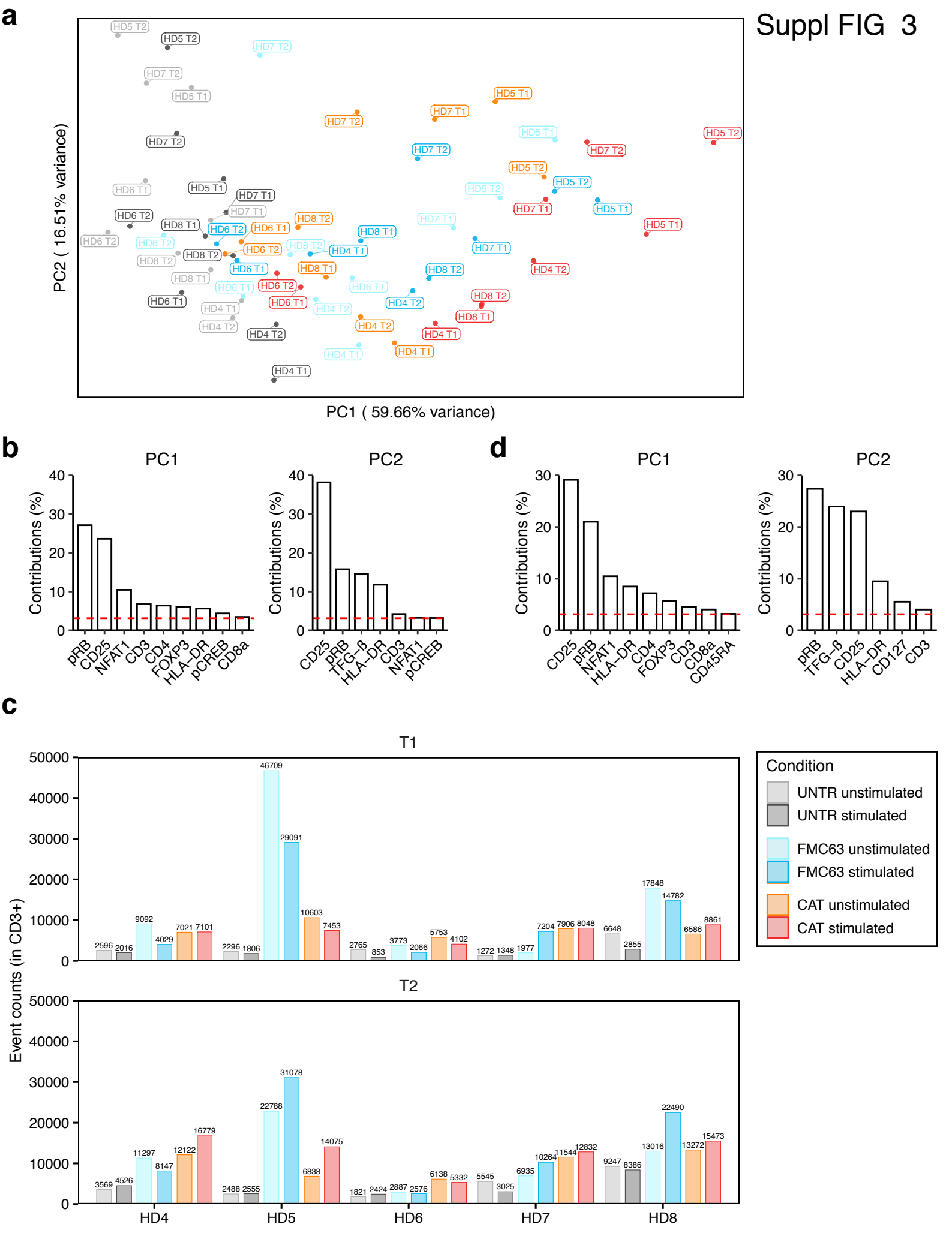
a
PC2 (16.51% variance)
PC1 (59.66% variance)
b
PC1
PC2
Contributions (%)
pRB
CD25
NFAT1
CD3
CD4
FOXP3
HLA−DR
pCREB
CD8a
TFG−β
d
CD45RA
CD127
c
T1
T2
Event counts (in CD3+)
HD4
HD5
HD6
HD7
HD8
Condition
UNTR unstimulated
UNTR stimulated
FMC63 unstimulated
FMC63 stimulated
CAT unstimulated
CAT stimulated

Supplementary Fig. 3: Mass cytometry analysis of unstimulated and stimulated untransduced and CAR-transduced T-cells.

a PCA plot of EMD scores from unstimulated and stimulated untransduced and CAR-transduced CD3+ T-cells at 3 h (T1) and 24 h (T2) post-stimulation (n= 5 HDs, n = 1 independent experiment). The labels specify each individual donor and the timepoint of the analysis, the colours identify each experimental condition.

b Bar plots of the top contributing variables to PC1 and PC2 in Fig. 2d. The dashed horizontal red line represents the expected average contribution of the variables.

c Bar plots showing the event counts in CD3+ T-cells measured for each sample. Samples are grouped by donor and the number of cells is displayed on top of the bars (n= 5 HDs, n = 1 independent experiment.

d Bar plots of the top contributing variables to PC1 and PC2 in panel a. The dashed horizontal red line represents the expected average contribution of the variables.

a-d Each experimental condition is indicated by a specific colour code (Unstimulated conditions = UNTR light grey, FMC63 light blue, CAT orange; stimulated conditions = UNTR grey, FMC63 blue, CAT red).

Suppl FIG 4

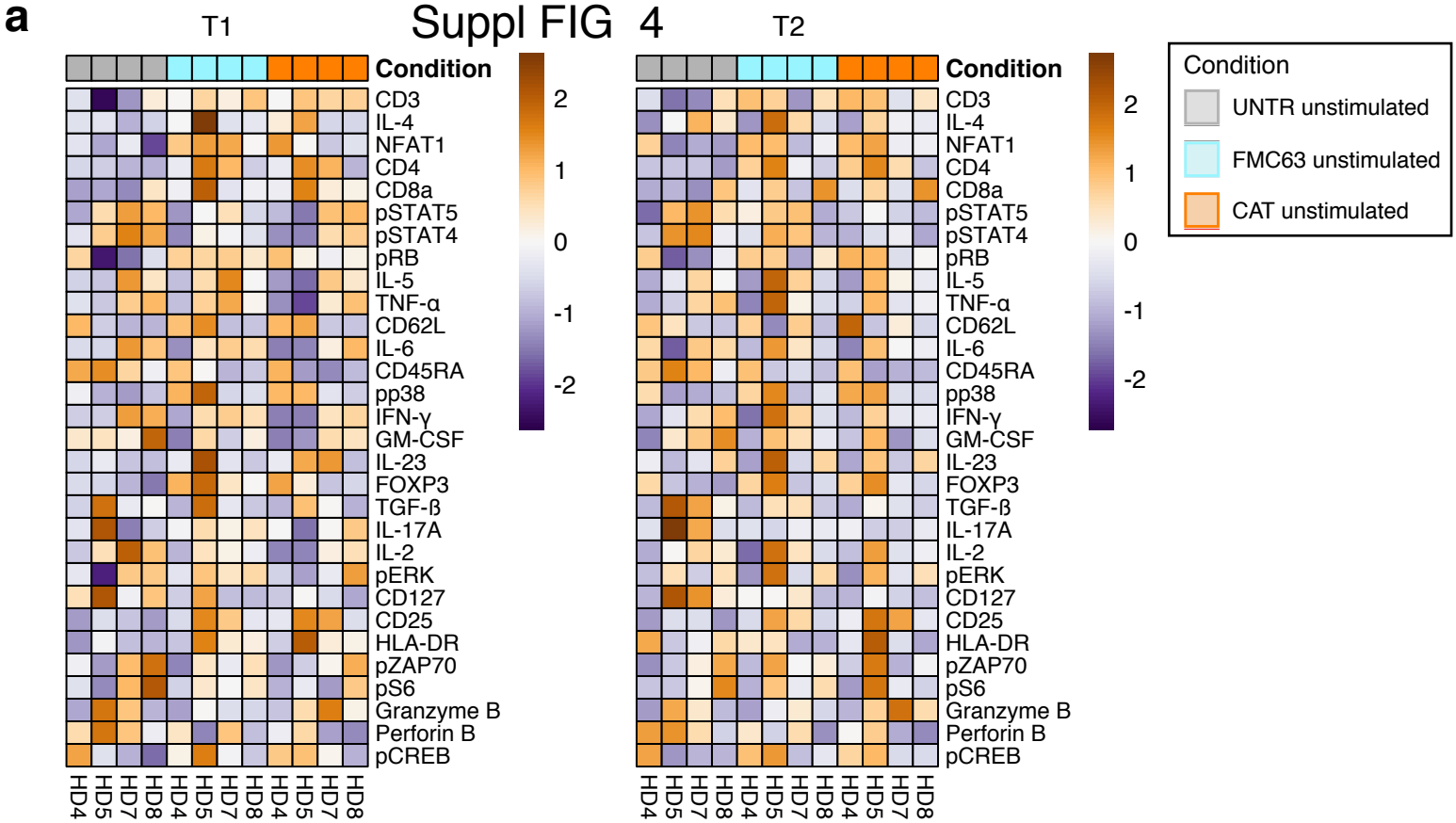
a
T1
T2
Condition
CD3
IL-4
NFAT1
CD4
CD8a
pSTAT5
pSTAT4
pRB
IL-5
TNF-α
CD62L
IL-6
CD45RA
pp38
IFN-γ
GM-CSF
IL-23
FOXP3
TGF-ß
IL-17A
IL-2
pERK
CD127
CD25
HLA-DR
pZAP70
pS6
Granzyme B
Perforin B
pCREB
HD4
HD5
HD7
HD8
2
1
0
-1
-2
Condition
UNTR unstimulated
FMC63 unstimulated
CAT unstimulated

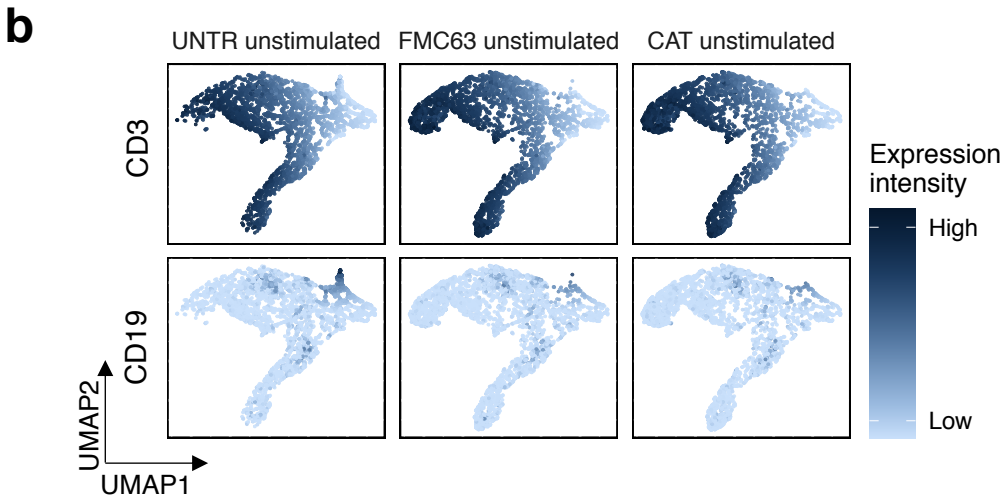
b
UNTR unstimulated
FMC63 unstimulated
CAT unstimulated
CD3
CD19
UMAP2
UMAP1
Expression intensity
High
Low

Supplementary Fig. 4: Molecular characterisation of unstimulated CAR-transduced T-cells.

a (left) Heatmap showing mass cytometry EMD scores computed at T1 (3 h stimulation) and (right) T2 (24 h stimulation) in CD3+ cells across all the unstimulated experimental conditions (n = 4 HDs, n = 1 independent experiment).

Each condition is indicated by a specific colour code (UNTR light grey, FMC63 light blue, CAT orange).

b UMAP showing the expression of selected markers (CD3, CD19) detected by mass cytometry at T2 (24 h stimulation) in unstimulated CD3+ cells across all the experimental conditions (n = 4 HDs, n = 1 independent experiment). The colour scale reflects the protein expression levels.

Suppl FIG 5

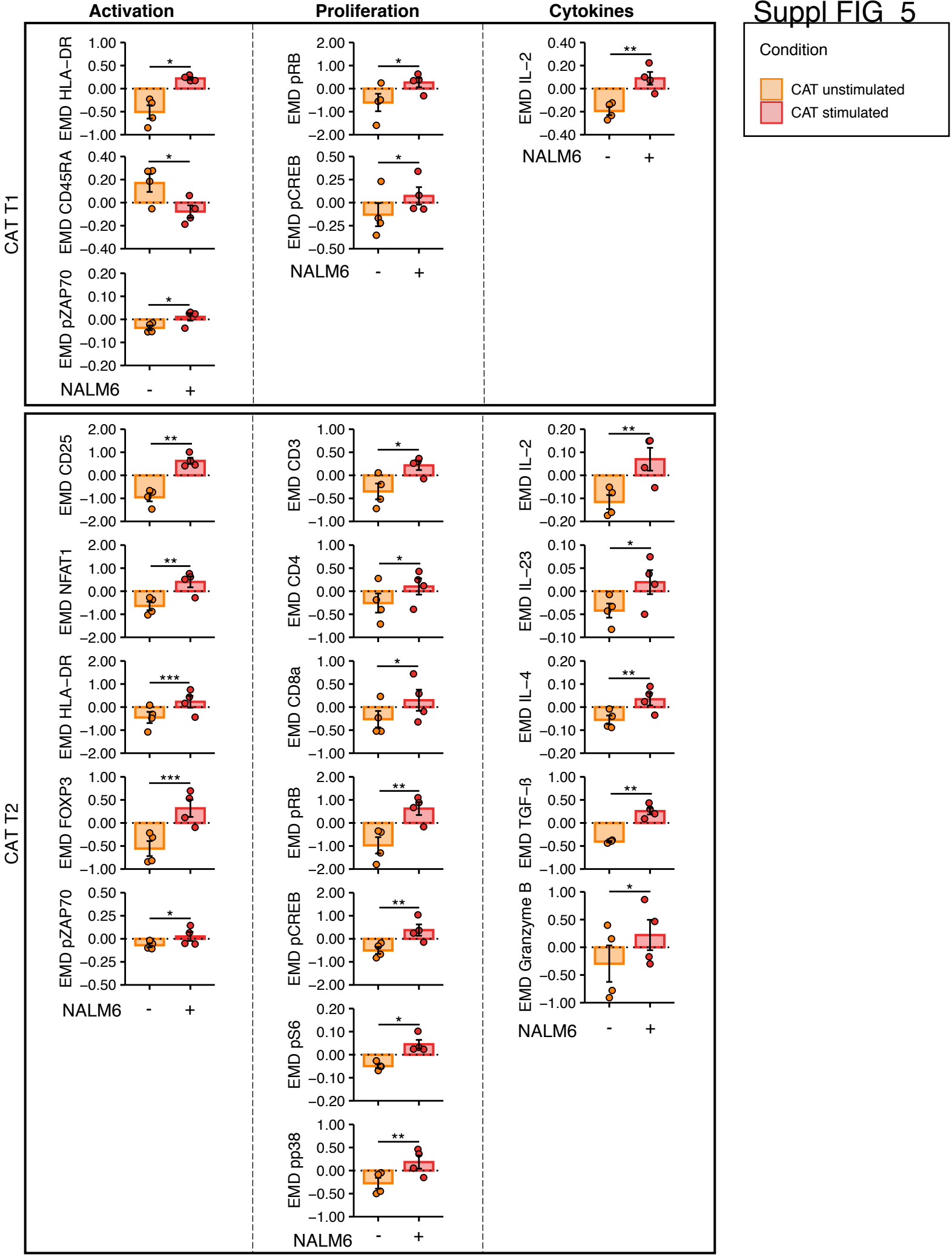
Activation
Proliferation
Cytokines
Condition
CAT unstimulated
CAT stimulated
CAT T1
EMD HLA−DR
EMD CD45RA
EMD pZAP70
EMD pRB
EMD pCREB
EMD IL−2
NALM6
CAT T2
EMD CD25
EMD NFAT1
EMD HLA−DR
EMD FOXP3
EMD pZAP70
EMD CD3
EMD CD4
EMD CD8a
EMD pRB
EMD pCREB
EMD pS6
EMD pp38
EMD IL−2
EMD IL−23
EMD IL−4
EMD TGF−ß
EMD Granzyme B

Supplementary Fig. 5: Mass cytometry EMD scores in unstimulated and stimulated CAT CAR-transduced T-cells.

(top) The barplots show mass cytometry EMD scores for activation/proliferation markers and cytokines differentially expressed between unstimulated and stimulated CAT CAR T-cells at T1 (3 h stimulation) and (bottom) at T2 (24 h stimulation). The dotted horizontal line (0) represents the average expression of a specific marker across all the experimental conditions analysed. (n = 4 HDs, n = 1 independent experiment).

Data represent mean ± se. Statistical significance was calculated by Paired t-test. *$P < 0.05$, **$P < 0.01$, ***$P < 0.001$.

Each experimental condition is indicated by a specific colour code (Unstimulated condition orange; stimulated condition red).

Suppl FIG 6

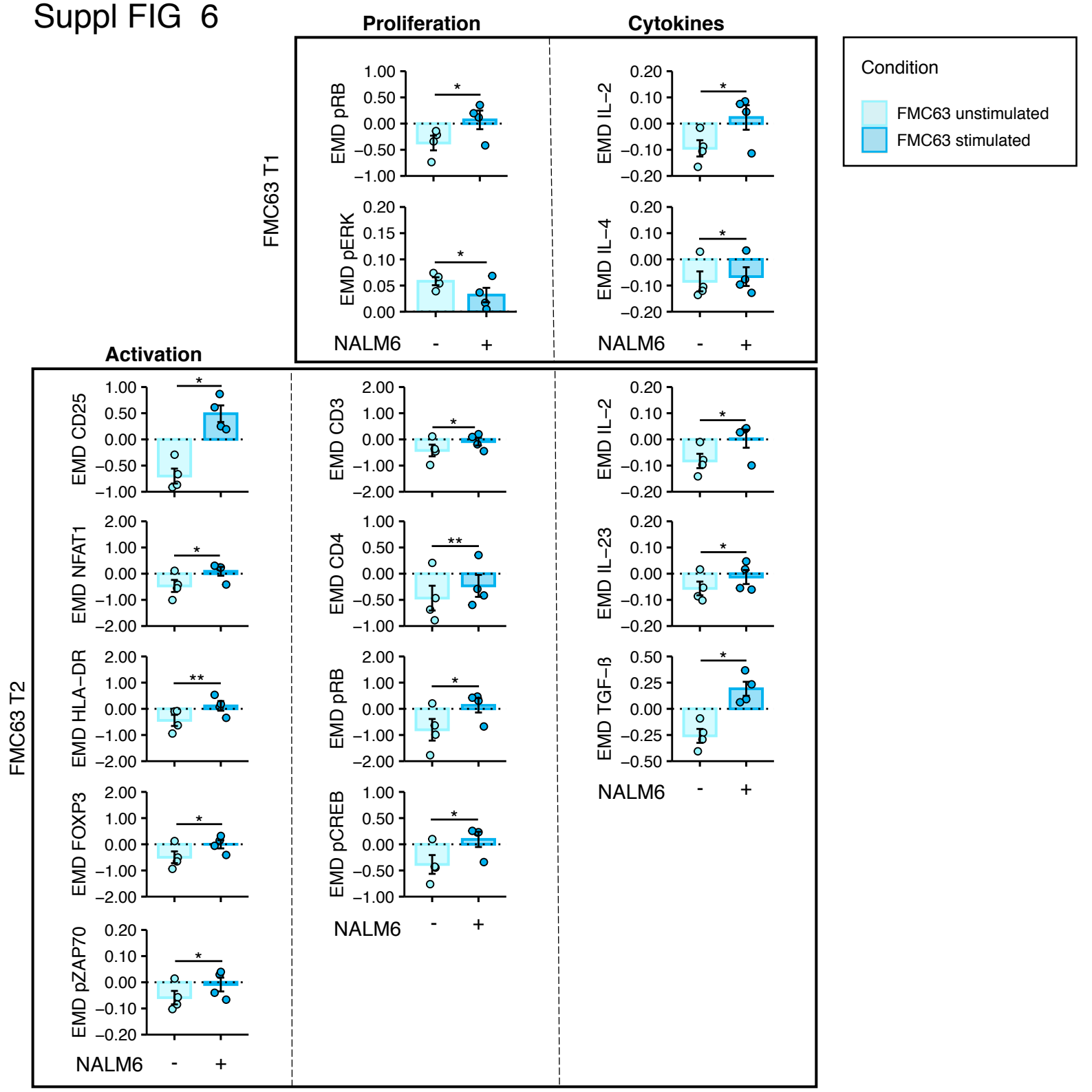
Proliferation
Cytokines
Activation
FMC63 T1
FMC63 T2
EMD pRB
EMD pERK
EMD IL−2
EMD IL−4
EMD CD25
EMD NFAT1
EMD HLA−DR
EMD FOXP3
EMD pZAP70
EMD CD3
EMD CD4
EMD pRB
EMD pCREB
EMD IL−2
EMD IL−23
EMD TGF−β
NALM6 - +
Condition
FMC63 unstimulated
FMC63 stimulated

Supplementary Fig. 6: EMD scores in unstimulated and stimulated FMC63 CAR-transduced T-cells.

(top) The barplots show mass cytometry EMD scores for activation/proliferation markers and cytokines differentially expressed between unstimulated and stimulated FMC63 CAR T-cells at T1 (3 h stimulation) and (bottom) at T2 (24 h stimulation). The dotted horizontal line (0) represents the average expression of a specific marker across all the experimental conditions analysed. (n = 4 HDs, n = 1 independent experiment).

Data represent mean ± se. Statistical significance was calculated by Paired t-test. *$P < 0.05$, **$P < 0.01$. Each experimental condition is indicated by a specific colour code (Unstimulated condition light blue; stimulated condition blue).

Suppl FIG 7

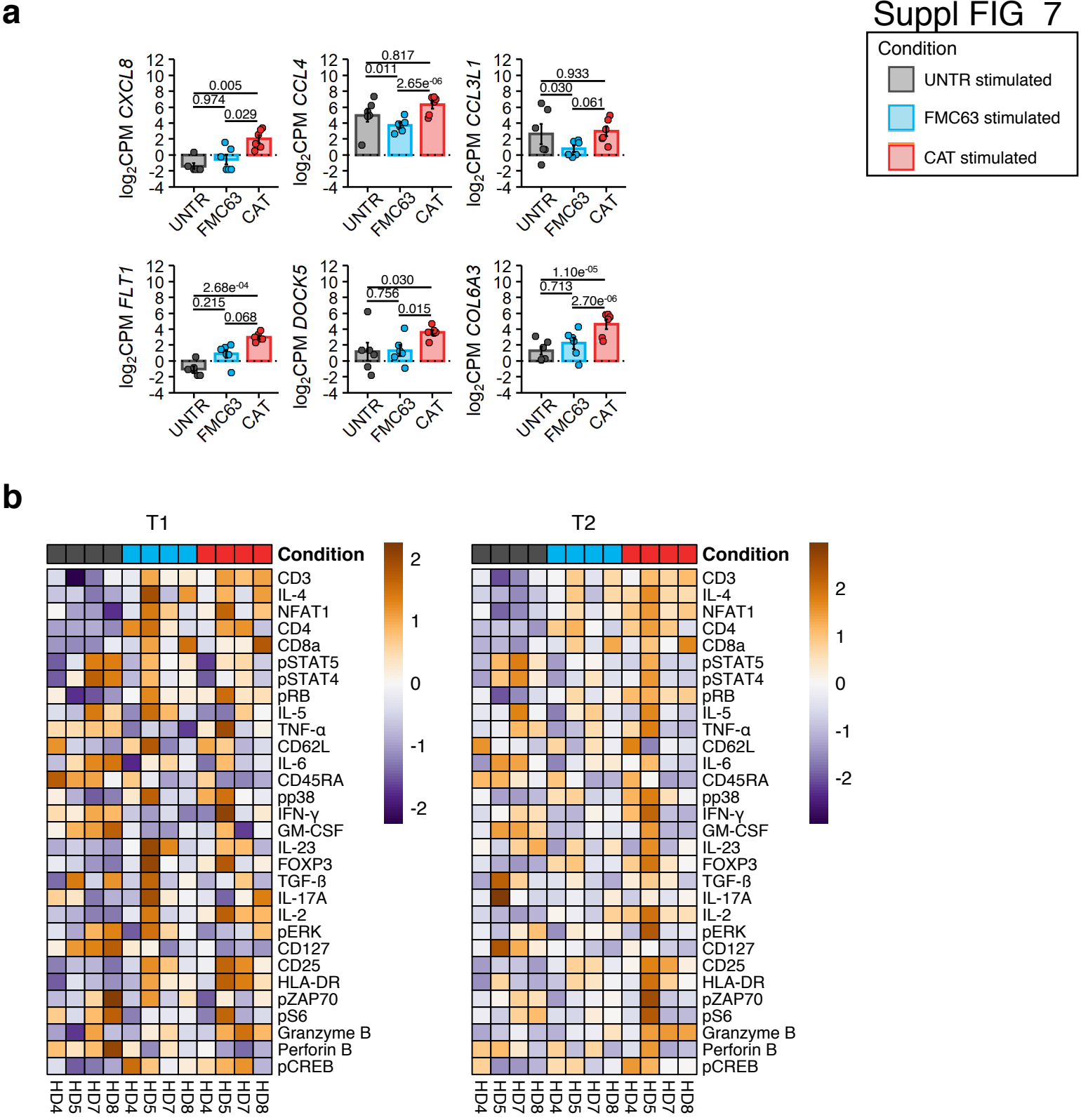
a
Condition
UNTR stimulated
FMC63 stimulated
CAT stimulated
log2CPM CXCL8
0.005
0.974
0.029
log2CPM CCL4
0.817
0.011
2.65e-06
log2CPM CCL3L1
0.933
0.030
0.061
log2CPM FLT1
2.68e-04
0.215
0.068
log2CPM DOCK5
0.030
0.756
0.015
log2CPM COL6A3
1.10e-05
0.713
2.70e-06
UNTR
FMC63
CAT
b
T1
T2
Condition
CD3
IL-4
NFAT1
CD4
CD8a
pSTAT5
pSTAT4
pRB
IL-5
TNF-α
CD62L
IL-6
CD45RA
pp38
IFN-γ
GM-CSF
IL-23
FOXP3
TGF-ß
IL-17A
IL-2
pERK
CD127
CD25
HLA-DR
pZAP70
pS6
Granzyme B
Perforin B
pCREB
HD4
HD5
HD7
HD8

Supplementary Fig. 7: Molecular characterisation of stimulated CAR-transduced T-cells.

a The barplots show the expression of selected DE genes (FDR < 0.1) in stimulated untransduced and transduced T-cells (n = 6 HDs, n = 2 independent experiments).

b (left) Heatmap showing mass cytometry EMD scores computed at T1 (3 h stimulation) and (right) T2 (24 h stimulation) in CD3+ cells across all the stimulated experimental conditions (n = 4 HDs, n = 1 independent experiment).

Each experimental condition is indicated by a specific colour code (UNTR grey, FMC63 blue, CAT red).

Suppl FIG 8

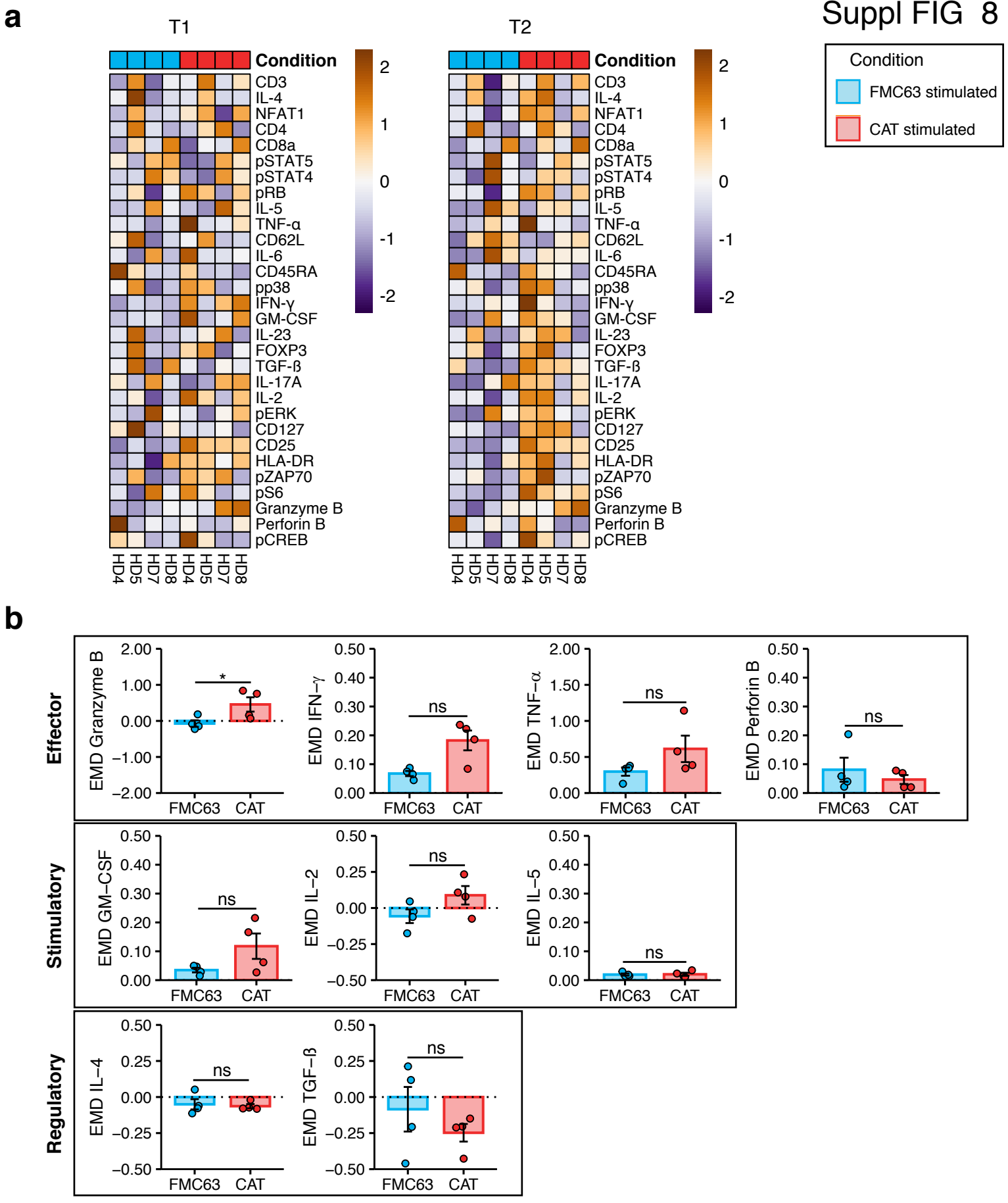
a
T1
T2
Condition
CD3
IL-4
NFAT1
CD4
CD8a
pSTAT5
pSTAT4
pRB
IL-5
TNF-α
CD62L
IL-6
CD45RA
pp38
IFN-γ
GM-CSF
IL-23
FOXP3
TGF-ß
IL-17A
IL-2
pERK
CD127
CD25
HLA-DR
pZAP70
pS6
Granzyme B
Perforin B
pCREB
HD4
HD5
HD7
HD8
2
1
0
-1
-2
Condition
FMC63 stimulated
CAT stimulated
b
Effector
Stimulatory
Regulatory
EMD Granzyme B
EMD IFN−γ
EMD TNF−α
EMD Perforin B
EMD GM−CSF
EMD IL−2
EMD IL−5
EMD IL−4
EMD TGF−ß
FMC63
CAT
*
ns

Supplementary Fig. 8: Molecular characterisation and cytokine expression of stimulated CAR-transduced T-cells.

a (left) Heatmap showing mass cytometry EMD scores computed at T1 (3 h stimulation) and (right) T2 (24 h stimulation) in stimulated FMC63 and CAT CAR T-cells (CD3+mCherry+).

b The barplots show the expression of mass cytometry EMD scores for selected effector (Granzyme B, IFN-γ, TNF-α, Perforin B), stimulatory (GM-CSF, IL-2, IL-5) and regulatory (IL-4 and TGF-β) cytokines in stimulated CAR T-cells at T1 (3 h stimulation). The dotted horizontal line (0) represents the average expression of a specific marker across all the experimental conditions analysed.

a-b Data represent mean ± se. Statistical significance was calculated by Paired t-test. *$P < 0.05$.

Each experimental condition is indicated by a specific colour code (UNTR grey, FMC63 blue, CAT red).

Suppl FIG 9

a

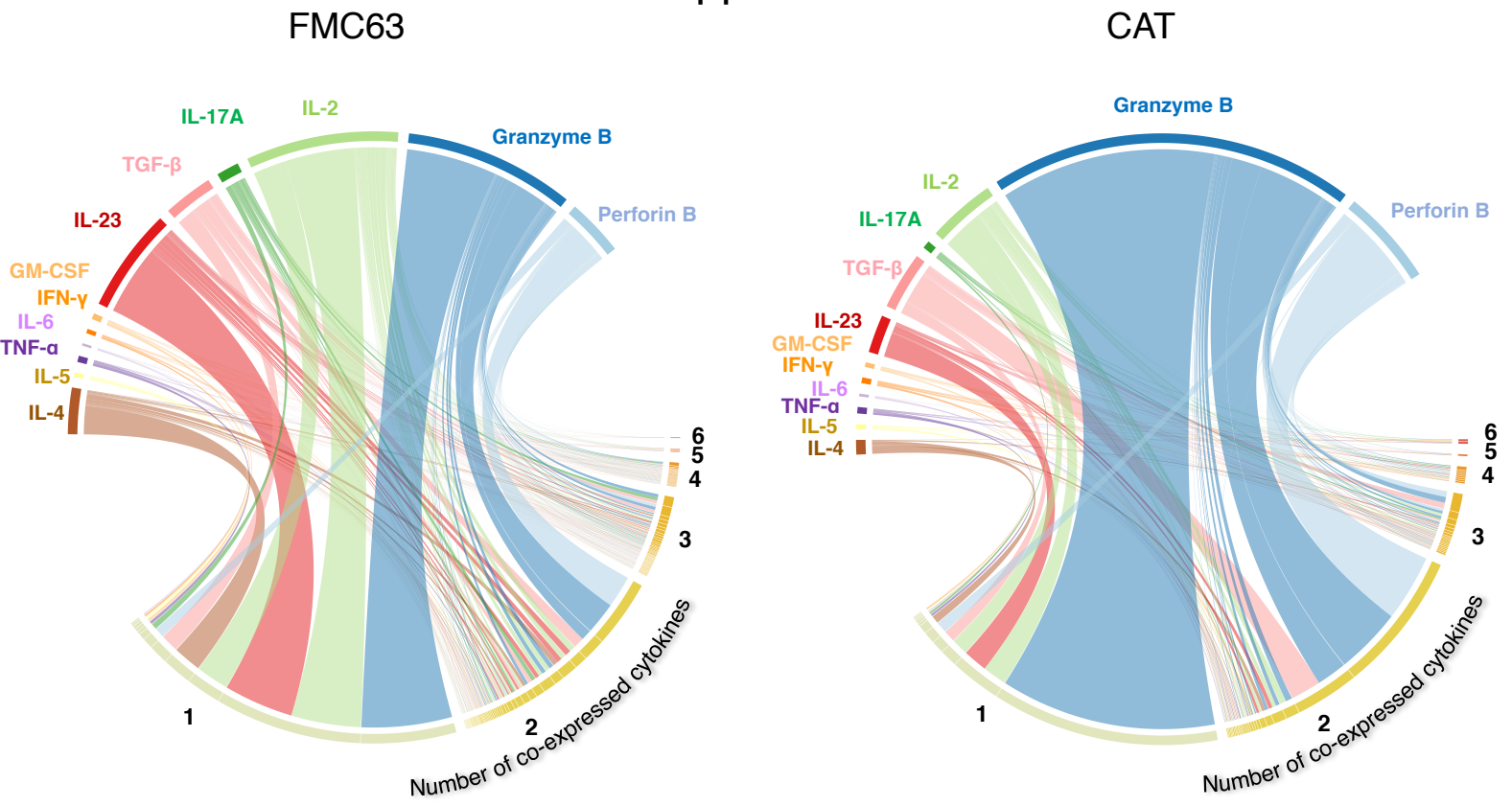

b

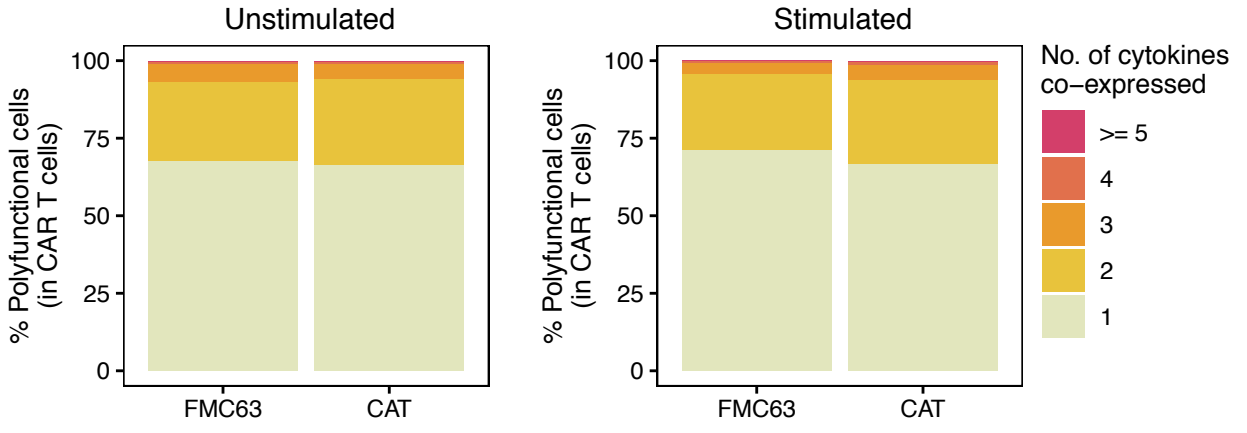

Supplementary Fig. 9: Cytokine polyfunctionality in stimulated CAR-transduced T-cells at 24 h post-stimulation.

a (left) The circos plots show all the combinations of the 12 cytokines analysed in stimulated FMC63 and (right) CAT CAR T-cells at T2 (24 h stimulation) by mass cytometry. A specific colour code has been assigned to each cytokine. The numbers indicate the frequencies of different patterns of cytokine co-expression (from 1 to 6 cytokines/cell).

b (left) The stacked barplots show the percentage of stimulated and unstimulated (right) CAR T-cells (CD3+mCherry+) expressing 1 to 4 or >=5 cytokines/cell at T2 (24 h stimulation) as measured by mass cytometry.

a-b n = 4 HDs, n = 1 independent experiment.

Suppl FIG 10

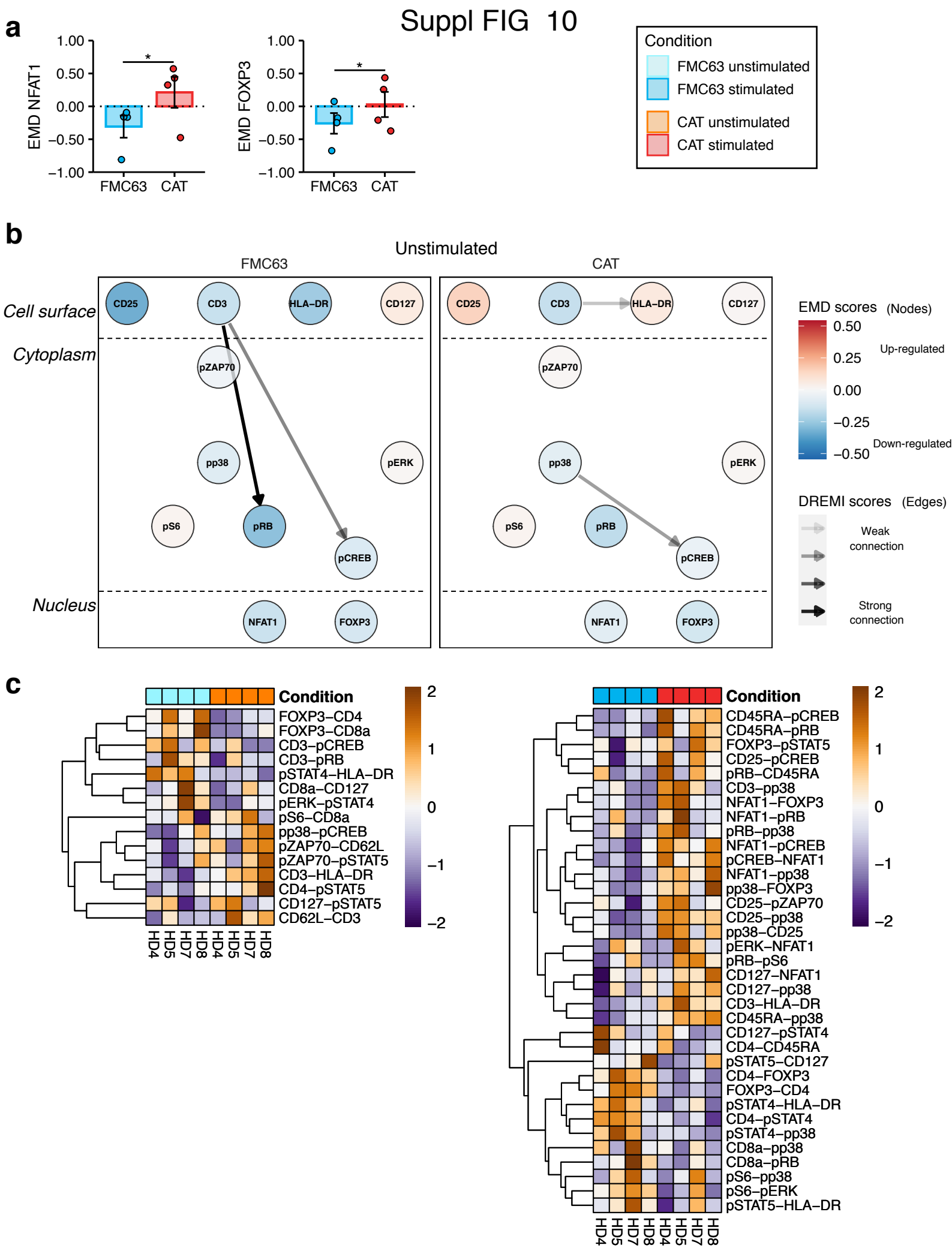
a
EMD NFAT1
EMD FOXP3
1.00
0.50
0.00
−0.50
−1.00
*
FMC63
CAT
Condition
FMC63 unstimulated
FMC63 stimulated
CAT unstimulated
CAT stimulated
b
Unstimulated
FMC63
CAT
Cell surface
Cytoplasm
Nucleus
CD25
CD3
HLA−DR
CD127
pZAP70
pp38
pERK
pS6
pRB
pCREB
NFAT1
FOXP3
EMD scores (Nodes)
0.50
0.25
0.00
−0.25
−0.50
Up-regulated
Down-regulated
DREMI scores (Edges)
Weak connection
Strong connection
c
Condition
FOXP3−CD4
FOXP3−CD8a
CD3−pCREB
CD3−pRB
pSTAT4−HLA−DR
CD8a−CD127
pERK−pSTAT4
pS6−CD8a
pp38−pCREB
pZAP70−CD62L
pZAP70−pSTAT5
CD3−HLA−DR
CD4−pSTAT5
CD127−pSTAT5
CD62L−CD3
HD4
HD5
HD7
HD8
2
1
0
−1
−2
Condition
CD45RA−pCREB
CD45RA−pRB
FOXP3−pSTAT5
CD25−pCREB
pRB−CD45RA
CD3−pp38
NFAT1−FOXP3
NFAT1−pRB
pRB−pp38
NFAT1−pCREB
pCREB−NFAT1
NFAT1−pp38
pp38−FOXP3
CD25−pZAP70
CD25−pp38
pp38−CD25
pERK−NFAT1
pRB−pS6
CD127−NFAT1
CD127−pp38
CD3−HLA−DR
CD45RA−pp38
CD127−pSTAT4
CD4−CD45RA
pSTAT5−CD127
CD4−FOXP3
FOXP3−CD4
pSTAT4−HLA−DR
CD4−pSTAT4
pSTAT4−pp38
CD8a−pp38
CD8a−pRB
pS6−pp38
pS6−pERK
pSTAT5−HLA−DR
HD4
HD5
HD7
HD8
2
1
0
−1
−2

Supplementary Fig. 10: Characterization of intracellular signalling in unstimulated and stimulated CAT and FMC63 CAR T-cells at 24 h post-stimulation.

a The barplots show the expression of mass cytometry EMD scores for NFAT1 and FOXP3 transcription factors in stimulated FMC63 and CAT CAR T-cells at T2 (24 h stimulation). The dotted horizontal line (0) represents the average expression of a specific marker across all the experimental conditions analysed. Barplots show mean ± se (n = 4 HDs, n = 1 independent experiment). Statistical significance was calculated by Paired t-test. *$P < 0.05$.

b Differential signalling network in unstimulated FMC63 and CAT CAR T-cells at T2 (24 h stimulation) post co-culture. The nodes are coloured by HD-averaged EMD scores computed between unstimulated CAR T-cells at T2 and arrows, whose transparency reflects HD-averaged DREMI scores, indicate differential markers connectivity between the 2 CAR products ($P <= 0.05$, n = 4 HDs, n = 1 independent experiment).

c (left) Heatmap showing mass cytometry DREMI scores differentially expressed in unstimulated and (right) stimulated FMC63 and CAT CAR T-cells at T2 (24 h stimulation) (n = 4 HDs, n = 1 independent experiment).

a-b Each condition is indicated by a specific colour code (unstimulated conditions = FMC63 light blue, CAT orange; stimulated conditions = FMC63 blue, CAT red).

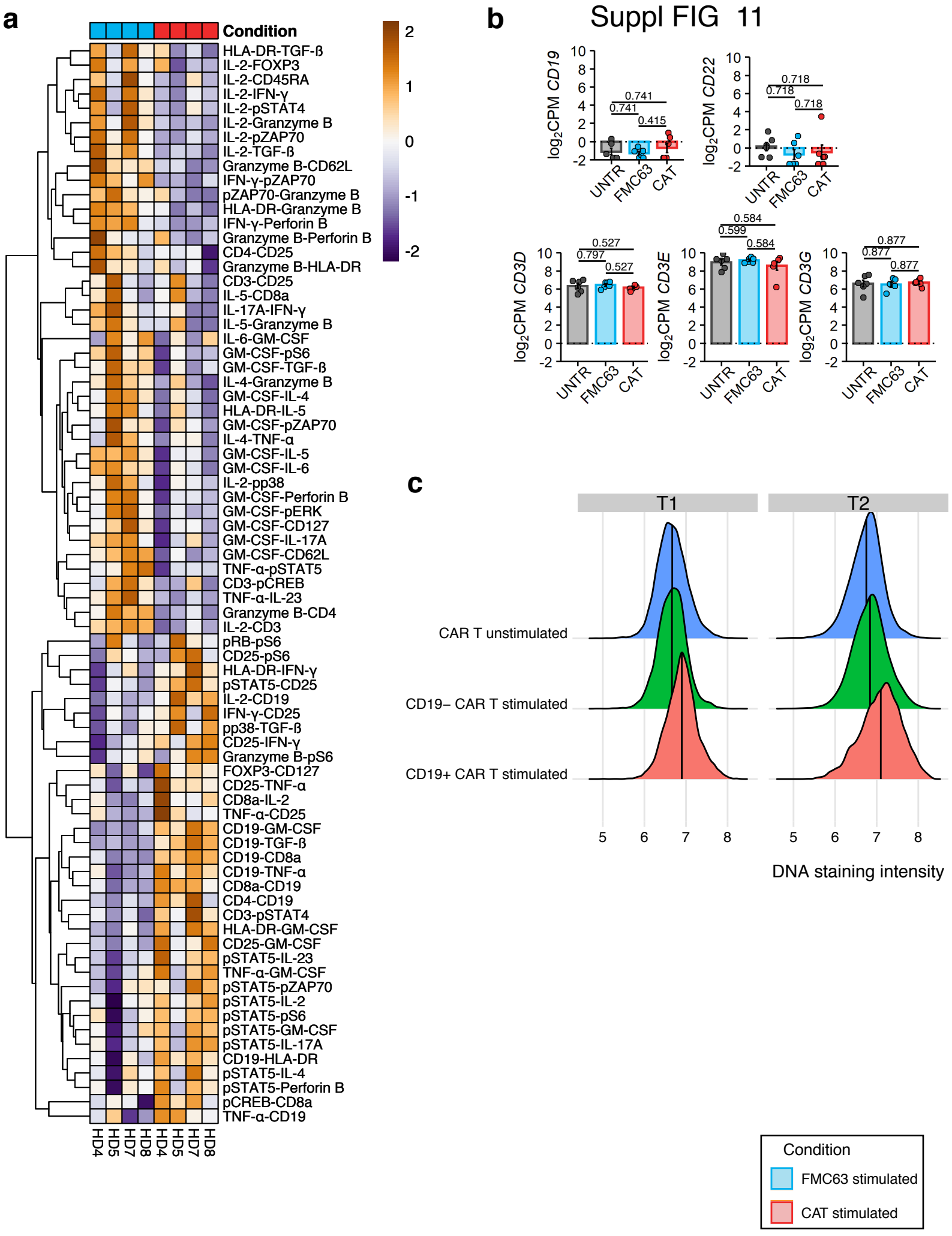
a
Condition
HLA-DR-TGF-ß
IL-2-FOXP3
IL-2-CD45RA
IL-2-IFN-γ
IL-2-pSTAT4
IL-2-Granzyme B
IL-2-pZAP70
IL-2-TGF-ß
Granzyme B-CD62L
IFN-γ-pZAP70
pZAP70-Granzyme B
HLA-DR-Granzyme B
IFN-γ-Perforin B
Granzyme B-Perforin B
CD4-CD25
Granzyme B-HLA-DR
CD3-CD25
IL-5-CD8a
IL-17A-IFN-γ
IL-5-Granzyme B
IL-6-GM-CSF
GM-CSF-pS6
GM-CSF-TGF-ß
IL-4-Granzyme B
GM-CSF-IL-4
HLA-DR-IL-5
GM-CSF-pZAP70
IL-4-TNF-α
GM-CSF-IL-5
GM-CSF-IL-6
IL-2-pp38
GM-CSF-Perforin B
GM-CSF-pERK
GM-CSF-CD127
GM-CSF-IL-17A
GM-CSF-CD62L
TNF-α-pSTAT5
CD3-pCREB
TNF-α-IL-23
Granzyme B-CD4
IL-2-CD3
pRB-pS6
CD25-pS6
HLA-DR-IFN-γ
pSTAT5-CD25
IL-2-CD19
IFN-γ-CD25
pp38-TGF-ß
CD25-IFN-γ
Granzyme B-pS6
FOXP3-CD127
CD25-TNF-α
CD8a-IL-2
TNF-α-CD25
CD19-GM-CSF
CD19-TGF-ß
CD19-CD8a
CD19-TNF-α
CD8a-CD19
CD4-CD19
CD3-pSTAT4
HLA-DR-GM-CSF
CD25-GM-CSF
pSTAT5-IL-23
TNF-α-GM-CSF
pSTAT5-pZAP70
pSTAT5-IL-2
pSTAT5-pS6
pSTAT5-GM-CSF
pSTAT5-IL-17A
CD19-HLA-DR
pSTAT5-IL-4
pSTAT5-Perforin B
pCREB-CD8a
TNF-α-CD19
HD4 HD5 HD7 HD8 HD4 HD5 HD7 HD8
2
1
0
-1
-2
b
Suppl FIG 11
log2CPM CD19
0.741
0.741
0.415
log2CPM CD22
0.718
0.718
0.718
log2CPM CD3D
0.527
0.797
0.527
log2CPM CD3E
0.584
0.599
0.584
log2CPM CD3G
0.877
0.877
0.877
UNTR
FMC63
CAT
c
T1
T2
CAR T unstimulated
CD19− CAR T stimulated
CD19+ CAR T stimulated
DNA staining intensity
Condition
FMC63 stimulated
CAT stimulated

Supplementary Fig. 11: Characterization of CD19-expressing CAR T-cells.

a Heatmap showing mass cytometry DREMI scores computed at T1 (3 h stimulation) in CD3+ CAR T-cells across all the stimulated experimental conditions.

b The barplots show the expression of B-cell (*CD19* and *CD22*)- and T-cell (*CD3D, E, G*)-related genes in stimulated untransduced and transduced T-cells. (n = 6 HDs, n = 2 independent experiments). The significance threshold is FDR < 0.1.

c Histograms showing the DNA marker intensity expression detected by mass cytometry at T1 (3 h stimulation), T2 (24 h stimulation) in unstimulated CAR T-cells and in stimulated trog- and trog+ CAR T-products.

a-c Each condition is indicated by a specific colour code (FMC63 blue, CAT red).

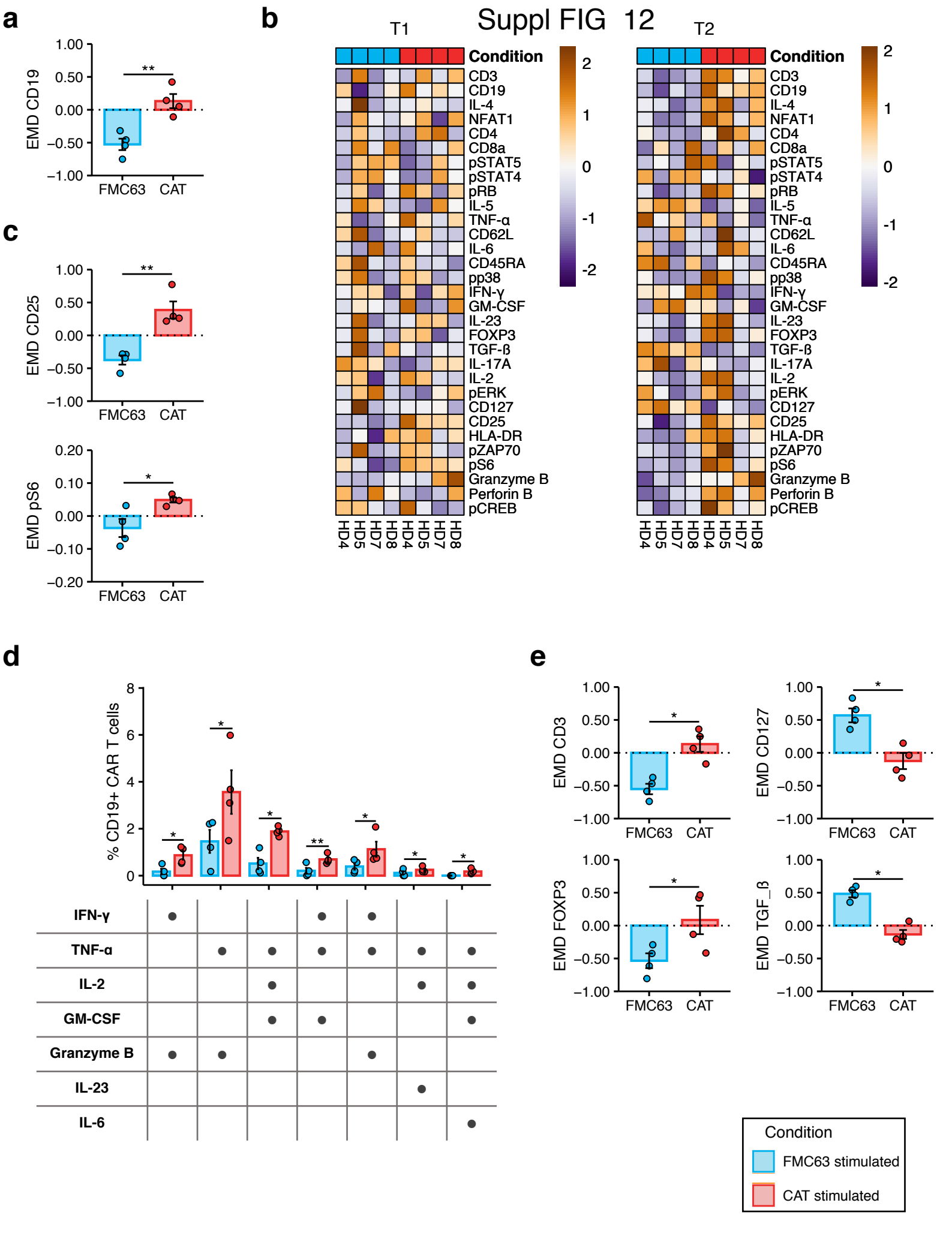
Suppl FIG 12
a
EMD CD19
FMC63
CAT
b
T1
T2
Condition
CD3
CD19
IL-4
NFAT1
CD4
CD8a
pSTAT5
pSTAT4
pRB
IL-5
TNF-α
CD62L
IL-6
CD45RA
pp38
IFN-γ
GM-CSF
IL-23
FOXP3
TGF-ß
IL-17A
IL-2
pERK
CD127
CD25
HLA-DR
pZAP70
pS6
Granzyme B
Perforin B
pCREB
HD4
HD5
HD7
HD8
c
EMD CD25
EMD pS6
d
% CD19+ CAR T cells
IFN-γ
TNF-α
IL-2
GM-CSF
Granzyme B
IL-23
IL-6
e
EMD CD3
EMD CD127
EMD FOXP3
EMD TGF_ß
Condition
FMC63 stimulated
CAT stimulated

Supplementary Fig. 12: Molecular characterisation of CAT and FMC63 CAR T-cells undergoing trogocytosis.

a The barplots show the expression of mass cytometry EMD scores for CD19 in stimulated FMC63 and CAT CAR T-cells at T2 (24 h stimulation). The dotted horizontal line (0) represents the average expression of a specific marker across all the experimental conditions analysed.

b (left) Heatmap showing mass cytometry EMD scores computed at T1 (3 h stimulation) and (right) at T2 (24 h stimulation) in trog+ CAR T-cells across all the stimulated experimental conditions.

c The barplots show the expression of mass cytometry EMD scores for CD25 and pS6 in stimulated FMC63 and CAT CAR T-cells at T1 (3 h stimulation). The dotted horizontal line (0) represents the average expression of a specific marker across all the experimental conditions analysed.

d The barplots show the percentage of the statistically different combinations of cytokines co-expressed in stimulated trog+ FMC63 and CAT CAR T-cells at T1 (3 h stimulation) by mass cytometry.

e The barplots show the expression of mass cytometry EMD scores for CD3, CD127, FOXP3 and TGF-ß in stimulated FMC63 and CAT CAR T-cells at T2 (24 h stimulation). The dotted horizontal line (0) represents the average expression of a specific marker across all the experimental conditions analysed.

a, c-e Barplots show mean ± se (n = 4 HDs, n = 1 independent experiment). Statistical significance was calculated by Paired t-test. *$P < 0.05$, ** $P<0.01$.

a-e Each condition is indicated by a specific colour code (FMC63 blue, CAT red).